Principles *and* Practice *of*
RADIATION ONCOLOGY

Third Edition

Edited by

Carlos A. Perez, M.D.
Director, Radiation Oncology Center
Mallinckrodt Institute of Radiology
Washington University Medical Center
St. Louis, Missouri

Luther W. Brady, M.D.
Hylda Cohn/American Cancer Society Professor of Clinical Oncology
and Professor, Department of Radiation Oncology
Allegheny University Hospitals-Hahnemann
Philadelphia, Pennsylvania

103 Additional Contributors

Assistants to the Editors
Connie Povilat
Alice Becker

Lippincott - Raven
PUBLISHERS
Philadelphia • New York

C

Acquisitions Editor: Stuart Freeman
Developmental Editor: Michelle LaPlante
Manufacturing Manager: Dennis Teston
Production Manager: Lawrence Bernstein
Production Editor: Jeffrey Gruenglas
Cover Designer: Jeane Norton
Indexer: Sandra King
Compositor: CJS Tapsco
Printer: Courier-Westford

3rd Edition

Printed in the United States of America

9 8 7 6 5 4 3 2 1

Library of Congress Cataloging-in-Publication Data

Principles and practice of radiation oncology/[edited by] Carlos A. Perez, Luther W. Brady; with 103 additional contributors; assistants to the editors, Connie Povilat, Alice Becker.—3rd ed.
p. cm.
Includes bibliographical references and index.
ISBN 0-397-58416-4
1. Cancer—Radiotherapy. I. Perez, Carlos A., 1934— II. Brady, Luther W., 1925—
[DNLM: 1. Neoplasms—radiotherapy. QZ 269 P957 1997]
RC271.R3P73 1997
616.99′40642—dc21
DNLM/DLC
for Library of Congress
97-3105
CIP

Principles and Practice of Radiation Oncology, Third Edition, edited by C. A. Perez and L. W. Brady. Lippincott–Raven Publishers, Philadelphia © 1997.

CHAPTER 1

Overview

Carlos A. Perez, Luther W. Brady, and Joseph L. Roti Roti

HISTORICAL PERSPECTIVE

The year 1995 marked the centennial of Roentgen's discovery of x-rays in 1895.[397] The Curies reported their discovery of radium in 1898.[91] Almost immediately, the biologic effects of ionizing radiations were recognized; the first patient cured by radiation therapy was reported in 1899, after which clinical radiation therapy had a challenging growth period in the early 1920s. Clinical and technologic advances accumulated more rapidly than did basic biologic knowledge.

Clinical radiation therapy as a medical discipline began at the International Congress of Oncology in Paris in 1922 when Coutard and Hautant presented evidence that advanced laryngeal cancer could be cured without disastrous, treatment-induced sequelae.[83] By 1934, Coutard[84] had developed a protracted, fractionated scheme that remains the basis for current radiation therapy, and in 1936 Paterson[343] published results in the treatment of cancer with x-rays. The use of brachytherapy, starting with ^{226}Ra needles and tubes, has increased steadily since 1910 in the treatment of malignant tumors in many anatomic locations. With time, ionizing radiation became more precise, high-energy photons and electrons were available, and treatment planning and delivery became more accurate and reproducible.

Knowledge of radiation physics, radiation biology, clinical treatment planning, and the use of computers in radiation therapy has grown exponentially. The last two decades have witnessed considerable advances in the treatment of cancer, with cure now being a realistic therapeutic objective in over 50% of newly diagnosed patients.[99,411] This improvement in therapy can be attributed to progress in several major areas:

1. Greater dissemination of information to physicians and the public and innovative screening and diagnostic tools that increase awareness and early cancer detection.
2. Multiple therapeutic approaches for a variety of tumors.
3. Advanced surgical and irradiation techniques and more effective cytotoxic drugs.
4. Greater interaction among cancer surgeons, radiation oncologists, medical oncologists, and pathologists, stressing the combined-modality approach in treatment.
5. Closer interaction among physicians and basic scientists, allowing the transfer of clinically relevant biomedical discoveries to the bedside.
6. Broad use of clinical trial methodology to evaluate new therapeutic strategies.

RADIATION ONCOLOGY IN CANCER MANAGEMENT

Radiation oncology is a clinical and scientific discipline devoted to management of patients with cancer and other diseases by ionizing radiation, alone or combined with other modalities, investigation of the biologic and physical basis of radiation therapy, and training of professionals in the field. *Radiation therapy* is a clinical modality dealing with the use of ionizing radiations in the treatment of patients with malignant neoplasias (and occasionally benign diseases). The aim of radiation therapy is to deliver a precisely measured dose of irradiation to a defined tumor volume with as minimal damage as possible to surrounding healthy tissue, resulting in eradication of the tumor, a high quality of life, and prolongation of survival at competitive cost.

In addition to curative efforts, radiation therapy plays a major role in cancer management in the effective palliation or prevention of symptoms of the disease: pain can be alleviated, luminal patency restored, skeletal integrity preserved, and organ function reestablished with minimal morbidity in a variety of clinical circumstances.[80]

In 1962, Buschke[48] defined a radiotherapist as a physician whose practice is limited to radiation therapy; he emphasized the active role of the radiation oncologist:

> While the patient is under our care we take full and exclusive responsibility, exactly as does the surgeon who takes care of a patient with cancer. This means that we examine the patient personally, review the microscopic material, perform examinations and take a biopsy if necessary. On the basis of this thorough clinical investigation we consider the plan of treatment and suggest it to the referring physician and to the patient. We reserve for ourselves the right to an independent opinion regarding diagnosis and advisable therapy and if necessary, the right of disagreement with the referring physician. . . . During the course of treatment, we ourselves direct any additional medication that may be necessary . . . and are ready to be called in an emergency at any time.

Buschke went on to indicate that, in order to integrate the various disciplines and provide better care to patients, it is extremely important for the radiation therapist (now oncologist) to cooperate closely with specialists in other fields in the management of the patient.

These concepts were reinforced and amplified by Bush[49] in his dissertation on "The Compleat Oncologist" and del Regato[97] in his 1975 ASTR presidential address.

Today radiation oncology is recognized as a separate specialty by the American Board of Radiology, the American College of Radiology, the American Board of Medical Specialties, the American College of Radiation Oncology, and the American Medical Association.

THE PROCESS OF RADIATION THERAPY

The clinical use of irradiation is a complex process that involves many professionals and a variety of interrelated functions (Fig. 1–1). The aim of therapy should be defined at the onset of the formulation of therapeutic strategy as follows:

	KEY STAFF	SUPPORTIVE ROLE
1. CLINICAL EVALUATION	Rad. Oncologist	
2. THERAPEUTIC DECISION	Rad. Oncologist	
3. TARGET VOLUME LOCALIZATION		
Tumor Volume	Rad. Oncologist	Sim. Tech./Dosimetrist
Sensitive Critical Organs	Rad. Oncologist	Sim. Tech./Dosimetrist
Patient Contour	Dosimetrist	Sim. Tech./Dosimetrist
4. TREATMENT PLANNING		
Beam Data-Computerization	Physicist	
Computation of Beams	Physicist	Dosimetrist
Shielding Blocks, Treatment Aids, etc.	Dosimetrist/ Mold Room Tech.	Rad. Oncologist/ Physicist
Analysis of Alternate Plans	Rad. Oncologist/ Physicist	Dosimetrist
Selection of Treatment Plan	Rad. Oncologist/ Physicist	
Dose Calculation	Dosimetrist	Physicist
5. SIMULATION/VERIFICATION OF TREATMENT PLAN	Rad. Oncologist/ Sim. Tech.	Dosimetrist/ Physicist
6. TREATMENT		
First Day Set-Up	Rad. Oncologist/ Physicist/ Therapy Techs.	Dosimetrist/ Physicist
Localization Films	Rad. Oncologist/ Therapy Techs.	
Dosimetry Checks/ Initial Chart Review	Physicist/ Rad. Oncologist	Dosimetrist/ Chief Tech.
Repositioning/Retreatment	Therapy Techs.	Dosimetrist/ Chief Tech.
7. PERIODIC EVALUATION (During Treatment)		
Tumor Response/Tolerance	Rad. Oncologist	Nurses/RTTs
8. FOLLOW-UP EVALUATION	Rad. Oncologist	Nurses

FIGURE 1–1. Functions involved in radiation therapy. (Inter-Society Council for Radiation Oncology: Radiation Oncology in Integrated Cancer Management. Philadelphia, PA, American College of Radiology, 1986)

1. *Curative,* in which it is projected that the patient has a probability of long-term survival after adequate therapy, even if that chance is low (as in T4 tumors of the head and neck or carcinoma of the lung).
2. *Palliative,* in which there is no hope of the patient surviving for extended periods; nevertheless symptoms that produce discomfort or an impending condition that may impair the comfort or self-sufficiency of the patient require treatment.

In curative therapy a certain probability of significant side effects of therapy, even though undesirable, may be acceptable. However, the same is not generally true in palliative treatment, in which no major iatrogenic conditions should be seen. Nevertheless, it is necessary to remember that in the palliation of primary tumors, relatively high doses of irradiation (sometimes 75% to 80% of curative dose) are required to control the tumor for the survival period of the patient.

In a curative setting it is extremely important for the radiation oncologist to deliver the highest possible dose to the tumor volume to ensure maximum tumor control, while keeping at the lowest possible level any severe sequelae of radiation treatment in the surrounding normal tissues. The prescription of irradiation is based on the following principles:

1. Evaluation of the full extent of the tumor (staging) by whatever means available, including radiographic, radioisotope, and other studies.
2. Knowledge of the pathologic characteristics of the disease, including potential areas of spread, that may influence choice of therapy (ie, rationale for elective irradiation of the lymphatics in the neck or pelvis).
3. Definition of goal of therapy (cure versus palliation).
4. Selection of appropriate treatment modalities, which may be irradiation alone or irradiation combined with surgery, chemotherapy, or both. The choice will have a significant impact on the volume treated and the doses of irradiation delivered.
5. Determination of the optimal dose of irradiation and the volume to be treated, which are made according to the anatomic location, histologic type, stage, potential regional nodal involvement, and other characteristics of the tumor, and the normal structures present in the region. The radiation oncologist should never hesitate to modify established policies in order to tailor the treatment plan to the needs of the patient.
6. Evaluation of the patient's general condition, periodic assessment of tolerance to treatment, tumor response, and status of the normal tissues treated.

The radiation oncologist must work closely with the physics, treatment planning, and dosimetry staffs to ensure the greatest possible accuracy, practicality, and cost benefit in the design of treatment plans and computation of dose distributions. The ultimate responsibility for treatment decisions and the technical execution of the therapy, as well as its consequences, will always rest with the radiation oncologist.[344] No computer calculations or physics procedures will correct the errors of clinical judgment, misunderstanding of physical concepts, or unsatisfactory planning and execution of radiation therapy. The skills of the clinician will never be completely replaced by technologic developments in physics, computers, or other technical aspects of radiation therapy; however, more accurate techniques and quality assurance procedures will ensure that the best possible treatment is being executed and that the possibility of subjective interpretations or inaccuracies is reduced to a minimum.

IRRADIATION TREATMENT PLANNING

It should be stressed that different doses of radiation are required for given probabilities of tumor control, depending on the type and initial number of clonogenic cells present. Therefore, varying radiation doses may be delivered to certain portions of the tumor (periphery versus central portion) or in cases in which all gross tumor has been surgically removed.[143]

From a cell burden standpoint, a clinical tumor can be considered to encompass several compartments: macroscopic (visible or palpable), microextensions into adjacent tissues, and subclinical disease, presumed to be present but not detectable even under the microscope. Treatment portals must adequately cover all three compartments in addition to a margin to compensate for geometric inaccuracies during irradiation exposure.

According to International Commission on Radiation Units and Measurements (ICRU) No. 50,[222] volumes of interest in treatment planning are defined as follows. Gross tumor volume (GTV) is all known gross disease including abnormally enlarged regional lymph nodes. When GTV is determined, it is important to use the appropriate computed tomography (CT) window and level settings that give the maximum dimension of what is considered potential gross disease. The clinical target volume (CTV) encompasses the GTV plus regions considered to harbor potential microscopic disease. The planning target volume (PTV) provides a margin around the CTV to allow for variation in treatment setup and other anatomic motion during treatment such as respiration. The PTV does not account for treatment machine beam characteristics (Fig. 1–2).[361,362]

Sensitive structures within the irradiated volume should be clearly identified, and the maximum doses and fractionation to be delivered to them must be specified. Simulation has been used in most instances to accurately identify the tumor volume and sensitive structures and to document the configuration of the portals and target volume to be irradiated.[114]

Perez and associates[362] described the conceptual struc-

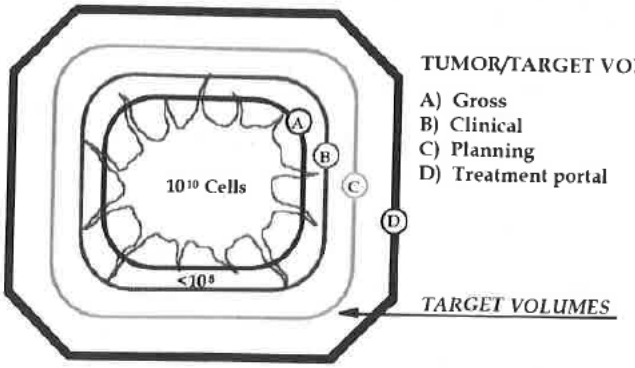

FIGURE 1–2. Schematic representation of "volumes" in radiation therapy. The treatment portal volume includes the tumor volume, potential areas of local and regional microscopic disease around the tumor, and a margin of surrounding normal tissue. (Modified from Perez CA, Purdy JA: Rationale for treatment planning in radiation therapy. In Levitt SH, Khan FM, Potish RA, ed: Levitt and Tapley's Technological Basis of Radiation Therapy: Practical Clinical Applications, ed 2. Philadelphia, PA, Lea & Febiger, 1992)

ture and process of a fully integrated three-dimensional (3-D) CT simulator. The elements of an optimal device include (a) volumetric definition of tumor volume and patient anatomy obtained with a CT scanner, (b) virtual simulation for beam setup and digitally reconstructed radiographs, (c) 3-D treatment planning for volumetric dose computation and plan evaluation, (d) patient-marking device to outline portal on patient's skin, and (e) verification (physical) simulation to verify portal placement on the patient. Average time for CT volumetric simulation was 74 minutes without or 84 minutes with contrast material. Average times were 36 minutes for contouring of tumor/target volume and 44 minutes for normal anatomy, 78 minutes for treatment planning, 53 minutes for plan evaluation/optimization, and 58 minutes for verification simulation. There were significant variations in time and effort according to the specific anatomic location of the tumor. Commercially available CT simulators lack some elements that were believed to be critical in a fully integrated 3-D CT simulator. Further efforts are in progress to develop more versatile and efficient 3-D simulators. Based on actual budgetary information, the cost of a volumetric CT simulation (separate from the 3-D treatment planning) showed that 1200 examinations per year (four to five per day in 250 working days) ideally should be performed to make the operation of the device cost effective.

Treatment aids, such as shielding blocks, molds, masks, immobilization devices, and compensators, are extremely important in treatment planning and delivery of optimal dose distribution. The radiation oncologist should be familiar with the physical characteristics of these devices and use them (although discriminately, for economic reasons) to achieve optimal therapeutic results. Simpler treatment delivery techniques that yield an acceptable dose distribution should be preferred over more costly and complex ones, in which a greater margin of error on a day-to-day treatment basis may be present. Repositioning and immobilization are critical because the only effective irradiation is that which strikes the clonogenic tumor cells. Therefore, in fractionated irradiation accurate setup should be such that the patient will maintain the desired position during every daily treatment. Repositioning and immobilization devices, such as the Alpha cradle, plaster casts, thermoplast molds, bite blocks, and arm boards, are invaluable in assisting technologists in patient positioning.

Accuracy is periodically assessed with portal (localization) films or on-line imaging verification (electronic portal imaging) devices.[296,484,502] Portal localization errors may be systematic or occur at random. On-line electronic portal imaging has been used to document inter- or intratreatment portal displacement in patients treated with pelvic irradiation.[484] Intertreatment displacement exceeding 10 mm was seen in 3% in the mediolateral, 16% in the craniocaudal, and 23% in the anteroposterior direction. There was no intratreatment displacement exceeding 10 mm in 547 images.

In a review of 48 patients on whom multiple digital portal verification images were obtained, Bissett and colleagues[36] noted that displacements of the field were 2.9 mm in the transverse and 3.4 mm in the craniocaudal dimensions. Mean rotational displacement was 2 degrees. The mean treatment field coverage in this set of images was 95%. There were some variations in the assessment of the translational errors when observations of several radiation oncologists were analyzed.

Rabinowitz and colleagues,[387] in a comparison of simulator and portal films of 71 patients, noted some discrepancies between the simulator and the localization (treatment) portal films. With an average value of 3-mm standard deviation of the variations, the mean worst case discrepancy averaged 3.5 mm in the head and neck region, 9.2 mm in the thorax, 5.1 mm in the abdomen, 8.4 mm in the pelvis, and 6.9 mm in the extremities. Other investigators have documented similar localization errors on the basis of portal film review analysis.[284,387]

TABLE 1–1. *Carcinoma of nasopharynx: correlation of quality of portal films with primary tumor control*

	Local tumor control			
	1956–1965 (n = 30)	1966–1975 (n = 54)	1976–1986 (n = 59)	Total (n = 143)
Simulation done	0	12/21 (57%)	43/57 (75%)	55/78 (71%)
Simulation not done	18/30 (60%)	16/33 (52%)	0	34/61 (56%)
				P = 0.1
>75% adequate portal films	8/11 (73%)	16/28 (57%)	42/56 (75%)	66/96 (69%)
<75% adequate portal films	10/19 (53%)	12/24 (50%)	1/1 (100%)	23/44 (52%)
				P = 0.07
Percent of films with ear block shielding nasopharynx				
≤25%	11/17 (65%)	22/36 (61%)	42/56 (75%)	75/109 (69%)
26–50%	7/12 (58%)	4/9 (44%)	1/1 (100%)	12/22 (55%)
>51%	0/1	2/7 (29%)	0/0	2/8 (25%)
				P = 0.04

(Perez CA, Devineni VR, Marcial-Vega V, et al: Carcinoma of the nasopharynx: Factors affecting prognosis. Int J Radiat Oncol Biol Phys 23:271–280, 1992)

Hendrickson[206] reported a 3.5% error frequency in multiple parameters (setting of field size, timer, gantry and collimator angles, and patient positioning) with one technologist working. The error rate declined to 0.82% when two technologists worked together. Marks and coworkers[284,285] demonstrated, by systematic use of verification films, a high frequency of localization errors in patients irradiated for head and neck cancer or malignant lymphomas. These errors were corrected with improved patient immobilization; with the use of a bite block in patients with head and neck tumors localization errors were reduced from 16% to 1%.[284]

Doss,[110] in a study of patients with upper airway carcinoma, showed that in 21 of 28 patients (75%) with treatments in which 30% or more portals exhibited a blocking error, a recurrence developed, whereas tumor failure was noted in only 2 of 12 patients (17%) without such errors.

Perez and colleagues[350] also reported a higher incidence of failures in patients with carcinoma of the nasopharynx on whom shielding of the ear inadvertently caused some blocking of tumor volume (Table 1–1).

Suit and associates[462] reviewed various recent technologic developments that through more precise treatment planning and delivery techniques will reduce volume irradiated and improve dose distributions, which should enhance therapeutic outcome.

RELEVANCE OF RADIOBIOLOGIC CONCEPTS IN CLINICAL RADIATION THERAPY

Clinical radiation therapy has evolved primarily from empiricism. Nevertheless, in the past 30 years a major effort has been applied to the potential application of radiobiologic concepts to design safer and more effective therapeutic strategies. Kaplan[234] pointed out that, although direct extrapolation from in vitro and in vivo experimental data may not have resulted in spectacular advances in clinical radiation therapy, these biologic concepts have greatly enhanced our understanding of the principles surrounding the clinical use of ionizing radiation. Experiments on radiation damage to DNA (both single- and double-strand scissions) and its repair have facilitated understanding of repair of sublethal and potentially lethal damage[125,520] and provided the rationale for manipulation of dose-time relationships.[149]

One of the most significant contributions of radiation biology has been the theory of cell kill as a function of increasing doses of a cytotoxic agent, as well as the demonstration of repair of sublethal or potentially lethal damage after irradiation.[126,382,520] These concepts have led to a better understanding of dose-response curves for tumor control probability and effect on normal tissues and application of dose-time concepts to fractionation. Studies on the role of oxygen and the demonstration of hypoxic cells in tumors and their impact on sensitivity to irradiation[378] was another important contribution leading to the concept of reoxygenation[232] and the potential use of hyperbaric oxygen or hypoxic radiation sensitizers in clinical radiation therapy.[103,516]

Höckel and associates[213] pointed out that tumor oxygenation measured with the polarographic needle electrode method was a powerful predictor of radiation therapy outcome in patients with locally advanced carcinoma of the uterine cervix. The 5-year survival rate was about 75% for 21 patients with a median pO_2 greater than 10 mm Hg versus 40% for 23 patients with a median pO_2 less than 10 mm Hg.

The study of cell proliferation kinetics, the biologic basis of cell killing by irradiation or chemotherapeutic agents, and the effectiveness of each modality in specific cellular compartments has strengthened understanding of combination therapy.[456,487,489] The same can be said for the use of various combinations of irradiation and surgery to decrease locoregional recurrences or to exploit the specific ability of each modality to eradicate tumor cells in

Principles and Practice of Radiation Oncology, Third Edition, edited by C. A. Perez and L. W. Brady. Lippincott–Raven Publishers, Philadelphia © 1997.

CHAPTER 8

Principles of Radiologic Physics, Dosimetry, and Treatment Planning

James A. Purdy

A solid foundation in the principles of radiologic physics, dosimetry, and treatment planning is essential for the practice of radiation oncology. In this chapter, we consider several topics that lay the basis for the material covered in Chapter 9. This chapter also discusses basic concepts used in calculating the dose administered to a patient and the standard correction methods used to account for air gaps and tissue inhomogeneities.

ATOMIC AND NUCLEAR STRUCTURE

The atom may be thought of as consisting of a centrally located core, the nucleus, surrounded by small orbiting particles, electrons. The overall dimension of the atom is about 10^{-10} m, the nucleus about 10^{-14} m. Most of the mass of the atom is contained in the nucleus, making it extremely dense (10^{15} kg/m^3). The nucleus is composed of two kinds of particles, protons and neutrons, known collectively as nucleons. A proton has a mass (m_p) of 1.673×10^{-27} kg and has a positive electrical charge equal in magnitude to the charge of the electron ($1.602 - 10^{-19}$ coulomb). Collectively, the protons constitute the electrical charge of the nucleus. A neutron is slightly more massive than a proton ($m_n = 1.675 \times 10^{-27}$ kg) and has no electrical charge. Each negatively charged electron has a rest mass (m_0) of 9.110×10^{-31} kg, contributing little mass to the nucleus.

In 1913, Niels Bohr formulated a planetary model of the hydrogen atom, consisting of an electron orbiting around a nucleus of equal and opposite charge. In extending his theory to multielectron atoms, Bohr proposed a nucleus surrounded by electrons arranged in concentric shells or energy levels (Fig. 8–1). Energy is released when an electron moves to an orbit closer to the nucleus, and energy is required to move an electron into a higher orbit. Historically, the shells are labeled, from innermost outward, by the letters K, L, M, and so forth. There is a maximum number of electrons that can be accommodated in each shell: two in the first shell, eight in the second, eighteen in the third, and so on.

The maximum number of electrons allowed in each shell is given by the relationship $2n^2$; n is an integer specific to each shell and is called the principal quantum number. Other properties of the electron also have discrete values specified by quantum numbers. These include the electron's angular momentum as it orbits the nucleus, denoted by quantum number l ($l = 0, 1, \ldots, n - 1$); its spin about its axis, denoted by s ($s = \pm 1/2$); and its magnetic moment, denoted by m_l ($m_l = 0, \pm 1, \ldots, \pm l$). Thus, each electron in an atom has an associated set of quantum numbers (n, l, s, m_l). This is the basis of the Pauli exclusion principle, which states that no two electrons can have the same set of quantum numbers within a particular atom.

Modern physics has replaced the simplistic orbiting electron model of Bohr with an abstract model of diffuse electron clouds that represent probability functions of the electron's position. However, for understanding of radiologic physics, the simple model of a nucleus composed of protons and neutrons and surrounded by electrons is sufficient.

The atom of an element is specified by its atomic number, denoted by the symbol Z, and its mass number, denoted by the symbol A. The atomic number is equal to the number of protons in the nucleus, and the mass number is equal to the number of nucleons (protons and neutrons) in the nucleus. Hence, A minus Z is equal to the number of neutrons, denoted by the symbol N, within the nucleus. In addition, each element has an associated chemical symbol. When these definitions are used, the standard notation to specify an atom is ${}^{A}_{Z}X$ as illustrated by ${}^{60}_{27}Co$, which is a radioactive isotope of the element cobalt that has an

an energetic photon approaches closely enough to the nucleus of the target atom, the incident photon energy may be converted directly into an electron–positron pair. Energy possessed by the photon in excess of 1.02 MeV appears as kinetic energy, which may be distributed in any proportion between the electron and the positron. When the positron comes to rest, it combines with an electron, and both particles then undergo mutual annihilation, with the appearance of two photons with energy of 0.511 MeV traveling in opposite directions.

The probability of pair production (π/ρ) occurring increases rapidly with incident photon energy above the 1.02-MeV threshold and is proportional to the second power of the atomic number of the target nuclei.

Photodisintegration

In photodisintegration, a high-energy photon interacts with the nucleus of an atom, totally disrupting the nucleus, with the emission of one or more nucleons (Fig. 8–15). It typically occurs at photon energies much higher than those encountered in radiation therapy.

Relative Importance of Interaction Processes

Figure 8–16 illustrates the relative importance of the photoelectric, Compton, and pair-production processes, three principal modes of interactions pertinent to radiation therapy, as a function of energy and atomic number of the absorber. For example, for an absorber with an atomic number approximately equal to that of tissue, 7, and for monoenergetichotons, the photoelectric effect is the dominant interaction below about 30 keV. Above 30 keV, the Compton effect becomes dominant and remains so until approximately 24 MeV, at which point pair production becomes the dominant interaction. The total mass attenuation coefficient is given by the sum of the individual coefficients

$$\mu_{en}/\rho = \sigma_{coh}/\rho + \tau/\rho + \sigma_c/\rho + \pi/\rho.$$

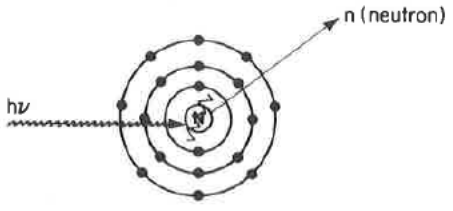

FIGURE 8–15. Schematic drawing illustrating the process of photodisintegration.

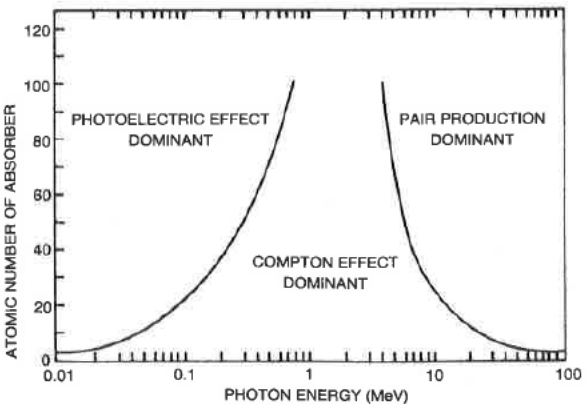

FIGURE 8–16. Relative importance of the three principal modes of interaction as a function of photon energy and atomic number of medium. (Hendee WR: Medical Radiation Physics, ed 2. Chicago, IL, Year Book Medical, 1979)

RADIATION THERAPY TREATMENT MACHINES

Kilovoltage Units

Before 1951, most radiation treatment units were x-ray machines capable of producing photon beams having only limited penetrability. In these machines, the electrons are accelerated by an electric field produced from a high voltage generated in a transformer that is applied directly between the filament (cathode) and the x-ray target (anode). A schematic diagram of a radiation therapy x-ray tube is shown in Fig. 8–17. The potential difference (kVp) is variable on these machines, and metal filters can be added to absorb the lower-energy photons preferentially, changing the penetrability of the beam. The combination of variable kVp and different filtration provides the capability of generating multiple x-ray beams. The degree of penetrability is used to categorize the units as

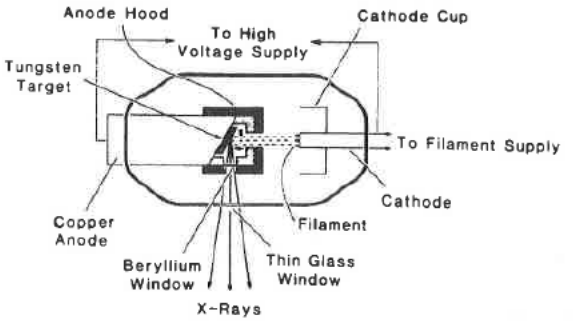

FIGURE 8–17. Schematic diagram of radiation therapy x-ray tube. (Khan FM: The Physics of Radiation Therapy, ed 3. Baltimore, Williams & Wilkins, 1994)

contact, superficial, and orthovoltage (deep-therapy) x-ray machines.

Contact Units

A contact x-ray machine typically operates at potentials of 40 to 50 kVp and at a tube current of 2 to 5 mA. Attached cones are used for a source–skin distance (SSD) of typically 2 cm or less. Filters of 0.5 to 1.0 mm aluminum are used to give a typical HVL of 0.6 mm aluminum. The primary radiation therapy application of a contact x-ray unit is for endocavitary irradiation of selected rectal carcinomas.[64,68] The x-ray tube is rod shaped with an extremely thin mica-beryllium window, having an inherent filtration of 0.03 mm aluminum equivalency, and the radiation is emitted axially.

Superficial Units

A superficial unit is an x-ray machine that operates at potentials of 50 to 150 kVp and 5 to 10 mA. Added thickness of filtration (1 mm Al to 1 mm Al + 0.25 mm Cu) produces HVLs of 1.0 to 8.0 mm of aluminum. Attached cones are typically used; lead masks are used to define irregular fields. The SSD is typically 15 or 20 cm. These machines are used primarily to treat skin lesions and are still in relatively widespread use.[38]

Orthovoltage (Deep-Therapy) Units

An orthovoltage unit is an x-ray machine that operates at potentials of 150 to 500 kVp. Most orthovoltage equipment operates between 200 and 300 kVp with tube currents of 10 to 20 mA. HVLs of 1 to 4 mm of copper are common with the use of added filters, such as the Thoreaus filter, a combination of sheets of tin, copper, and aluminum arranged so that the highest atomic number is always closest to the x-ray target, ensuring that the higher-energy characteristic x-rays are absorbed by the lower Z metal. Fields are usually defined by detachable cones. The SSD is typically 50 cm. Few of these machines are still used clinically.

Supervoltage and Megavoltage Photon and Electron Treatment Units

The first supervoltage machines were resonant transformer and Van de Graaff generator x-ray units operating at 1 to 2 MV. These machines are now obsolete and no longer in clinical use. A guide to the development and literature of these early accelerators used in medicine can be found in the review articles by Schulz[69] and Trout.[82]

^{60}Co Teletherapy Machines

The first ^{60}Co (telecobalt) machine was loaded with its source in August 1951 in the Saskatoon Cancer Clinic in Canada, and the first patient was treated in November of that year.[25]

The advantages of any radioactive isotope teletherapy machine are its constancy of beam intensity, predictability of decay with a well-defined half-life, and lack of day-to-day small-output fluctuations typically found in electrical machines. Most isocentric ^{60}Co machines use a source-to-axis distance (SAD) of 80 cm. Later models provide for 100 cm SAD with higher activity (10,000 Ci) sources. A typical design is illustrated in Fig. 8–18.

The high specific activity of ^{60}Co permits the fabrication of small, high-activity sources, typically 6000 to 7000 Ci in 1.5- to 2.0 cm diameter sources, giving dose rates of about 1.5 to 2 Gy/min at 80 cm when the source is new. Maximum field sizes of 40 × 40 cm at the treatment distance of 80 cm are now available on some newer machines. The penetration of the 1.17-MeV and 1.33-MeV γ-rays from ^{60}Co is such that the $d_{1/2}$ in tissue (the depth at which the dose has been reduced to 50% of the maximum dose value) is about 10 cm. Disadvantages of ^{60}Co units include the need for source replacement approximately every 4 to 5 years, poor field flatness for large fields, and lower depth dose compared with high-energy photons from linear accelerators.

Cobalt 60 teletherapy machines are becoming obsolete, partly from lack of technologic upgrades and partly from the demands of regulatory burden. Washington University's last ^{60}Co teletherapy machine was removed from clinical operation in 1995.

Betatron

The first betatron, developed by Kerst in 1941, produced x-rays of 2 MV.[30] Later models used in radiation oncology produced x-ray beams with energies of over 40 MV.[26,47] The betatron resembles a large electric power transformer. Electrons are accelerated by magnetic induction in an evacuated circular structure (doughnut). A magnetic field is produced by passing an alternating current through the primary windings or exciting coils of a large electromagnet. The electrons accelerate within the doughnut. A stream of electrons, when injected at the appropriate time in the magnetic induction cycle, follows an orbital path and remains in an equilibrium orbit for hundreds of thousands of revolutions in a fraction of a second. Only the first one quarter of the induction cycle is used in the acceleration, and the radiation is produced in pulses.

The production of the clinical beams is achieved by applying a contraction pulse to change the path of the electrons from the equilibrium orbit. When an x-ray beam is required, the accelerated electrons are made to strike a

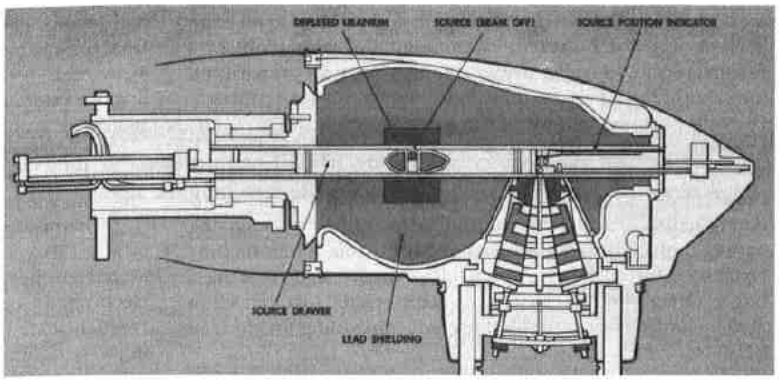

FIGURE 8–18. Schematic cutaway diagram showing ^{60}Co source head. (Courtesy of Atomic Energy Canada, Ltd)

metal target, producing bremsstrahlung x-rays. Otherwise, the electrons can be extracted through a thin metal window built into the doughnut, providing an electron beam for clinical use.

Because of small beam currents and thin target x-ray production, betatrons are low-intensity x-ray machines. The dose rate at 100 cm increases with energy from 0.25 Gy/min at approximately 15 MV to 0.9 Gy/min at 45 MV. Electron dose rates are typically much higher, ranging from 1 to 3 Gy/min. Because of the betatron's low-intensity x-ray dose rate, its field size is limited to no greater than about 20 × 20 cm at a treatment distance of 100 cm. Betatrons are usually heavy and bulky machines, but some, such as the Brown-Bovari machine, are isocentrically mounted, allowing moving beam therapy and the positioning of the beam at different orientations. The number of medical betatrons in clinical use has decreased significantly, and only a few, if any, are in operation.

Linear Accelerators

The first microwave electron linear accelerator (8 MV) for medical use became operational in 1953 at the Radiation Research Center of the Medical Research Council at Hammersmith Hospital in London.[48] The design for an isocentric gantry mount for the accelerator was first conceived by P. Howard-Flanders.[23] Shortly thereafter, Kaplan, Ginzton, and co-workers at Stanford developed a 6-MV medical linear accelerator (linac).[17] Since then, there have been continued advances in accelerator design and construction.[29] Linear accelerators now account for more than 75% of all operational megavoltage treatment units in the industrialized world.[29]

Figure 8–19 is a block diagram of a high-energy bent-beam medical linear accelerator showing the major components, auxiliary systems, and interconnections. The linear accelerator uses high-frequency electromagnetic waves to accelerate electrons to high energy through a microwave accelerator structure. The high-energy electron beam itself can be used for treating superficial tumors, or it can be made to strike a target to produce an x-ray beam for treating deep-seated tumors. Modern medical linear accelerators are designed so that the source of radiation can rotate around a horizontal axis (gantry axis). As the gantry rotates, the collimating axis moves in a vertical plane. The isocenter is the point of intersection of the collimator axis and the gantry axis.

The microwave accelerator structure consists of a stack

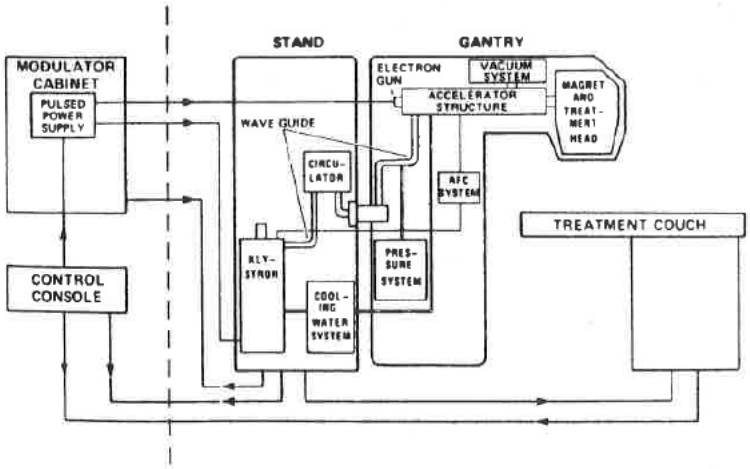

FIGURE 8–19. Schematic block diagram showing major components of high-energy bent-beam medical linear accelerator. (Courtesy of Varian Associates)

of cylindrical cavities having an axial hole through which the accelerated electrons pass. Medical linear accelerators accelerate electrons by traveling or standing electromagnetic waves of frequencies in the microwave region (3000 MHz). In the standing wave design, the microwave power is coupled into the structure by side-coupling cavities, rather than through the beam aperture. This design tends to be more efficient than the traveling wave design, but it can be more expensive. For further details on this subject and overall linear accelerator operation, the reader is referred to the textbook by Karzmark and associates.[29] The accelerator structure in low-energy linear accelerators is typically mounted in the treatment head collinear with the components associated with producing, controlling, and monitoring the x-ray beam. The magnetron or klystron and associated electronics, with the waveguide necessary to transmit the radio frequency power from the magnetron to the accelerator structure, are all situated within the gantry or connecting stand. The high-energy machines use a horizontally mounted accelerator structure with a beam-bending magnet system. Accelerator structure technology now makes possible two high–dose-rate photon beams of widely separated energy.

In the medical linear accelerator, the electrons are ejected with an initial energy of about 50 keV into the accelerator structure, where they interact with the electromagnetic field of the microwaves. The electrons are accelerated by the force of the electrical field associated with radio frequency waves. The electrons are carried along the radio frequency waves somewhat in the manner of a surfboard riding an ocean wave.

At the exit window of the accelerating structure, the high-energy electrons emerge in the form of a pencil beam of about 2 to 3 mm in diameter. In low-energy (4 to 6 MeV) medical linear accelerators having in-line short accelerating structure, the accelerated electrons proceed in a straight line and strike a target, producing bremsstrahlung x-rays. However, in high-energy medical linear accelerators, the accelerating structure is much longer and is placed horizontally or at some angle with respect to the horizontal, requiring that the electrons be bent through a suitable angle, usually 90 or 270 degrees between the accelerating structure and the target. This is enabled by the beam transport system, which consists of an achromatic focusing and bending magnet, as well as steering and focusing coils.

The angular distribution of x-rays produced by megavoltage electrons incident on a target is forward peaked. To make the x-ray beam intensity uniform across the field, a conical flattening filter is inserted in the beam. Filters have been constructed of lead, tungsten, uranium, steel, and aluminum (or some combination of these), depending on x-ray energy.

The flattened x-ray beam then passes through a monitor ionization chamber. This is typically a monitoring system that consists of several transmission-type parallel-plate ionization chambers, which cover the entire beam. These chambers are used to monitor the integrated dose, the field symmetry, and the dose rate.

After passing through the monitor chamber, the beam can be further collimated by continuously movable x-ray collimators, consisting of two pairs of lead or tungsten blocks (jaws), which provide a rectangular opening from zero to the maximum field size. In the newer units, independent jaw capability is available.

In the electron mode, the x-ray target is retracted and the pencil electron beam strikes an electron-scattering foil to broaden the beam and produce a flat field across the treatment field. The scattering-foil system typically consists of dual lead foils. The thickness of the first foil ensures that most of the electrons are scattered with only a minimum of bremsstrahlung x-rays. The second foil is generally thicker in the central region and is used to flatten the field. The bremsstrahlung produced appears as x-ray contamination of the electron beam and is typically less than 5% of the maximum. In some medical linear accelerators, the electron beam field flatness is accomplished by electromagnetic scanning of the electron pencil beam over the irradiated area rather than the use of scattering foils. A schematic diagram of beam subsystems for both x-ray and electron beams is shown in Fig. 8–20.

Microtrons

The microtron, whose concept is credited to Veksler, is an electron accelerator that combines the basic principles of the electron linear accelerator and the cyclotron.[84] By using magnets to recirculate the electron beam through a microwave accelerator cavity (or cavities) one or more times, a high-beam energy can be achieved with a low-energy accelerating section. After each orbit in the magnet, the electron bunch must arrive in phase with the accelerator microwave field. Thus, the magnet system acts as an energy spectrometer, limiting the electron energy acceptance to a narrow energy width and consequently limiting to some extent the beam current.

In the circular orbit microtron, electrons are accelerated as they pass through a microwave cavity and move in a uniform magnetic field, where they describe circular trajectories of increasing radius. Adjustments are made to the cavity voltage, frequency, and magnetic field so that the electrons always encounter the electric field of the microwave cavity in phase. The principles of operation are illustrated in Fig. 8–21.

Because of the very narrow energy spread of the electron beam, it is feasible to transport the beam from a centrally located microtron to two or more treatment rooms by relatively small focusing and bending magnets. The gantry in each treatment room is compact, containing only the beam transport magnets and the radiation head. However, only a few dual treatment room circular orbit microtron facilities have been built.

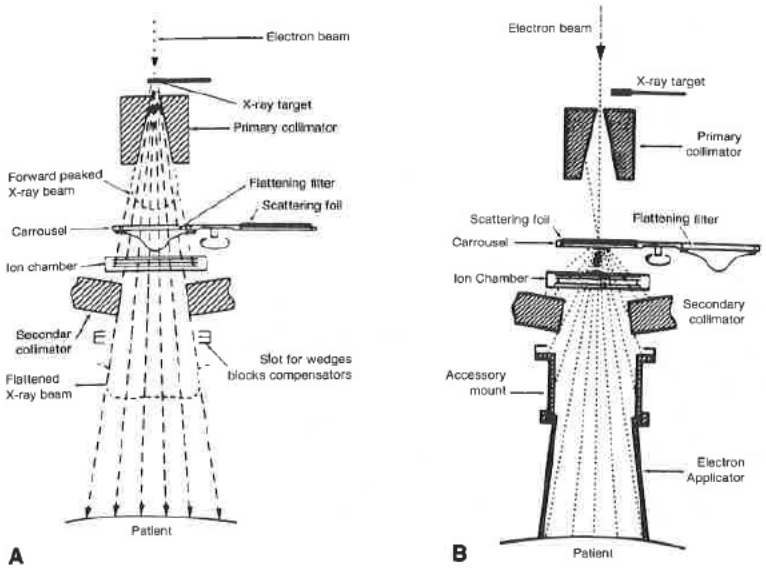

FIGURE 8–20. Schematic diagram of beam subsystems for (**A**) x-ray beam and (**B**) electron beam therapy. (Karzmark CJ, Morton RJ: A Primer on Theory and Operation of Linear Accelerators in Radiation Therapy. Reprinted with permission of the Department of Health and Human Services, Public Health Service, Food and Drug Administration, Bureau of Radiological Health, 5600 Fishers Lane, Rockville, MD 20857)

The racetrack microtron concept was first suggested by Schwinger in 1946.[70] It uses two D-shaped magnet pole pieces that are separated by a fixed distance, between which is a multicavity accelerator structure. This approach permits more energy gain per lap, hence fewer orbits for a given energy, smaller magnets, and a more compact machine. The principles of operation are illustrated in Fig. 8–22. Based on the Schwinger concept, Wernhoim and co-workers[66] at the Royal Institute of Technology, Stockholm, developed a racetrack microtron that produced a 50-MeV beam with a 3-MeV energy gain per orbit. A 50-MeV medical version of this machine has been developed by the Swedish firm Scanditronics.[6] A fully computer-controlled version (MM50) that can be

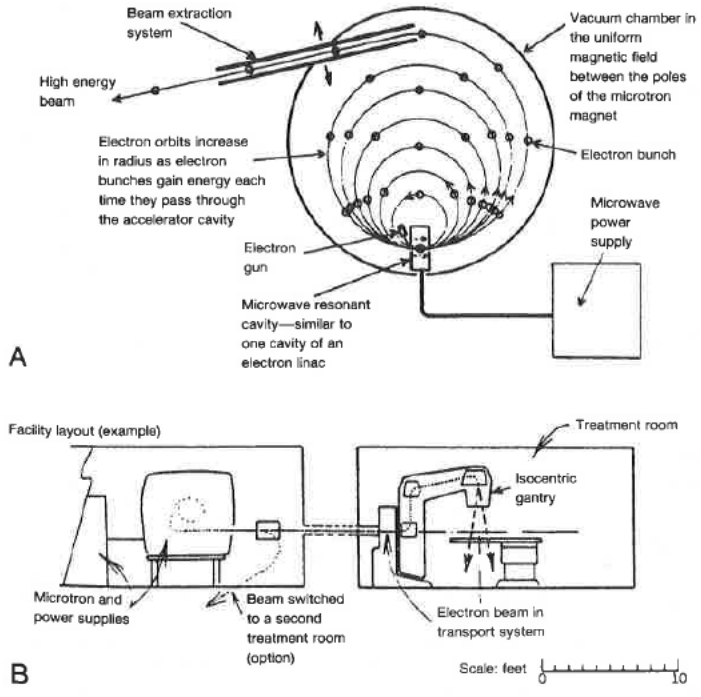

FIGURE 8–21. (**A**) Schematic drawing showing principles of circular microtron operation. (**B**) Medical characteristics. (Redrawn from Megavoltage radiation therapy equipment: A source document for the February 1981 Blue Book on Criteria for Radiation Oncology in Multidisciplinary Cancer Management. Philadelphia, American College of Radiology, 1983)

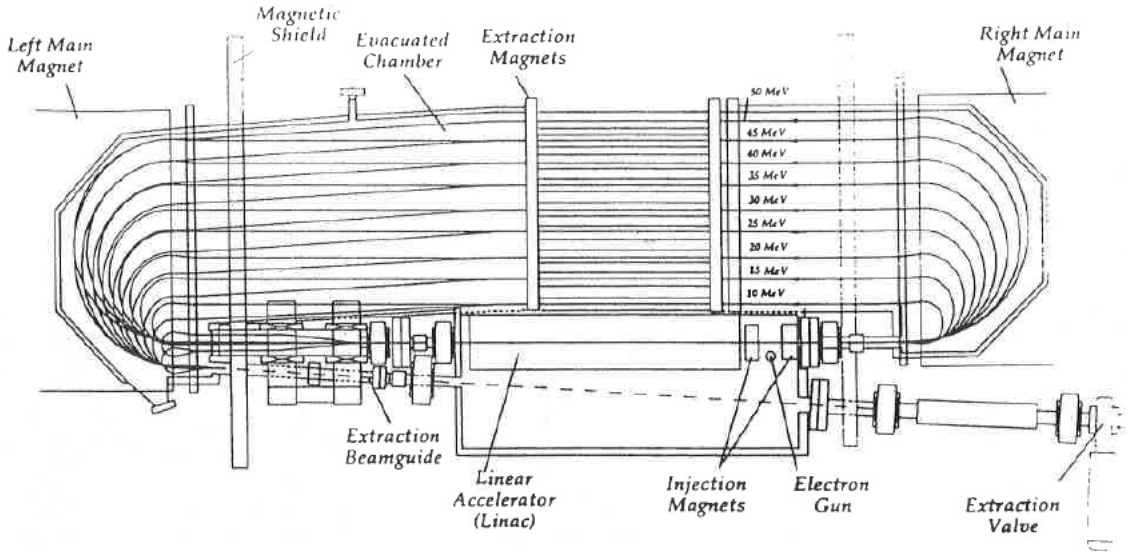

FIGURE 8–22. Schematic drawing showing principles of racetrack microtron. (Masterson ME, Mageras GS, LoSasso T, et al: Preclinical evaluation of the reliability of a 50 MeV racetrack microtron. Int J Radiat Oncol Biol Phys 28:1219–1227, 1994)

used in an automated multisegment mode has been installed at Memorial Sloan-Kettering Cancer Center and University of Michigan Medical Center.[15,41] Because of the high energy, the electron beam is scanned in both x-ray and electron modes. The principal virtues of the racetrack microtron are its compactness for high energy, transportability of the narrow energy spread beam by magnets, ease of changing energy over a wide range for both electron and x-ray beams, and need for only a relatively low-power microwave source to obtain rather high electron energies.

Proton Beam Treatment Units

The basic absorption characteristics of heavy charged particles including protons and heavy ions allow radiation treatment with dose distributions that are highly conformal with target volume shapes. Protons traverse relatively straight paths through a tissue medium, slowing down continuously by interactions with surrounding electrons and by occasional nuclear interactions. This results in depth-dose characteristics that show approximately constant dose over most of the beam range but increasing to a sharp Bragg peak at the end of the range as shown in Fig. 8–23. Dose at the peak is approximately four times the entrance dose, and the width of the peak is on the order of 1 cm, depending on beam energy and beam energy spread. Superposition of monoenergetic proton beams allows the customization of depth-dose characteristics for individual patients through the generation of spread out Bragg peaks that cover the target and decrease sharply to zero dose a few millimeters beyond the target (Fig. 8–24). The biologic effectiveness of proton beams is similar to other low linear energy transfer (LET) radiation.[19] Therefore, the clinical response data base established for photon and electron treatment is applicable to proton treatment.

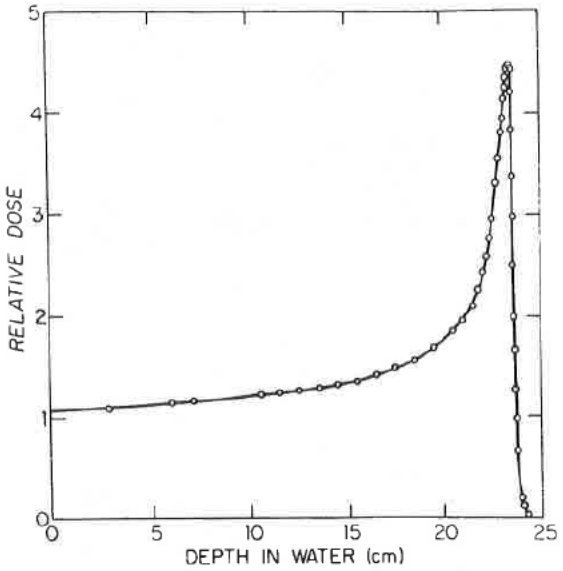

FIGURE 8–23. Depth dose distribution for 187-MeV protons from the Uppsala synchrocyclotron showing Bragg peak. The dose reaches a sharp peak at a depth of about 23 cm. (Hall EJ: Radiobiology for the Radiologist, ed 4. Philadelphia, JB Lippincott, 1994)

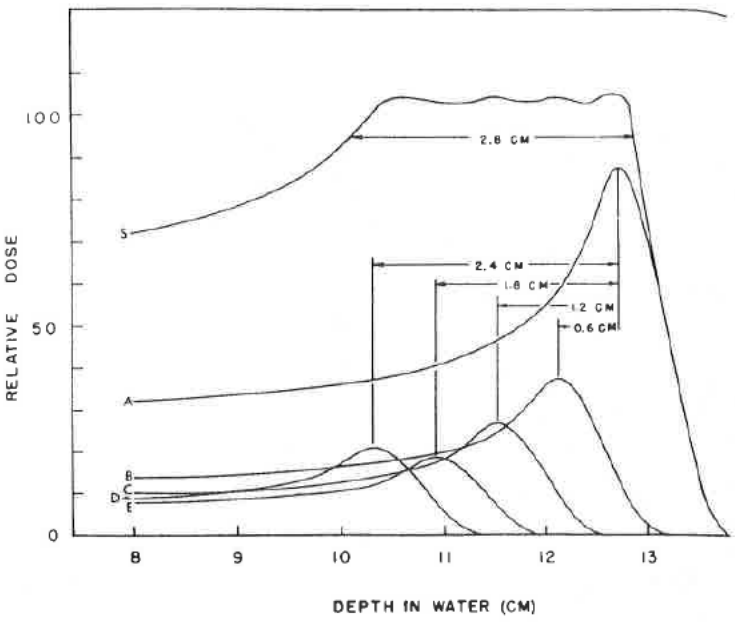

FIGURE 8–24. Drawing illustrating the way in which the Bragg peak for a proton beam can be spread out. Curve A is the depth-dose distribution for the primary beam of 160-MeV protons at the Harvard cyclotron. Beams of lower intensity and shorter range, as illustrated by curves B, C, D, and E, can be added to give a composite curve S, which results in a uniform dose over 2.8 cm. (Hall EJ: Radiobiology for the Radiologist, ed 4. Philadelphia, JB Lippincott, 1994)

The principal components of a proton radiation therapy treatment facility are the accelerator, a beam transport system for guiding the beam to one or more treatment rooms, and a beam delivery system to direct and shape the beam for individual patient treatments. In most existing or proposed proton treatment facilities, either a cyclotron or a synchrotron is used for the proton accelerator. The principles of the cyclotron and synchrotron are shown in Figs. 8–25 and 8–26. The synchrotron has the advantage of simple energy variability, whereas the cyclotron is capable of high beam intensity. The choice of accelerator type must be made considering every aspect of the treatment facility, including the intended beam delivery system, available space, and radiation shielding. First, the accelerator must provide a beam with sufficient energy to penetrate body tissues to the distal edge of the deepest intended target considering any energy losses in the beam spreading system. A proton beam energy of 250 MeV penetrates approximately 38 cm of water and is considered adequate for most radiation therapy applications. Beam intensity from the accelerator must be adequate to overcome losses in the beam delivery system and provide tolerable treatment times considering patient motion and facility throughput. Beam spreading is accomplished by scattering foil systems or dynamic beam scanning systems.

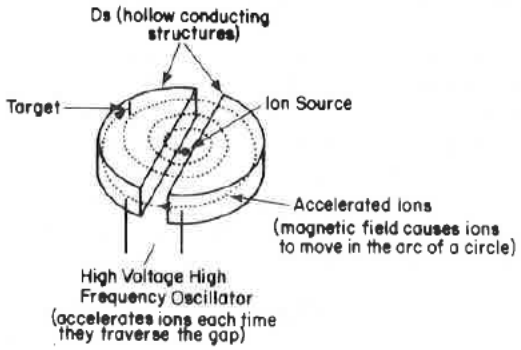

FIGURE 8–25. Schematic drawing showing principles of cyclotron operation. This machine is used for accelerating positive ions and is clinically used to produce proton and neutron beams. Metal half-disks (Ds) have an evacuated center through which the protons can travel. The protons are accelerated by an oscillating electric field operating between the half-disks. A magnetic field perpendicular to the plane of the half-disks confines the charged particles in the half-disks.

Three proton treatment facilities are presently operating within the United States: Harvard Cyclotron Laboratory, Loma Linda University Medical Center, and University of California at Davis. The Harvard Cyclotron Laboratory has provided treatment facilities for the Massachusetts General Hospital Radiation Medicine Department and others since 1961 and has treated over 6000 patients.[49] The cyclotron generates a 160-MeV proton beam that may be switched to provide fixed horizontal beams in either of two treatment rooms. A new proton beam therapy center is being built at the Massachusetts General Hospital.

In 1990, the Department of Radiation Sciences at Loma Linda University Medical Center opened the first dedicated, hospital-based proton treatment facility.[9] To date, they have treated over 1100 patients.[49] This center contains three treatment rooms with rotating gantries, a treat-

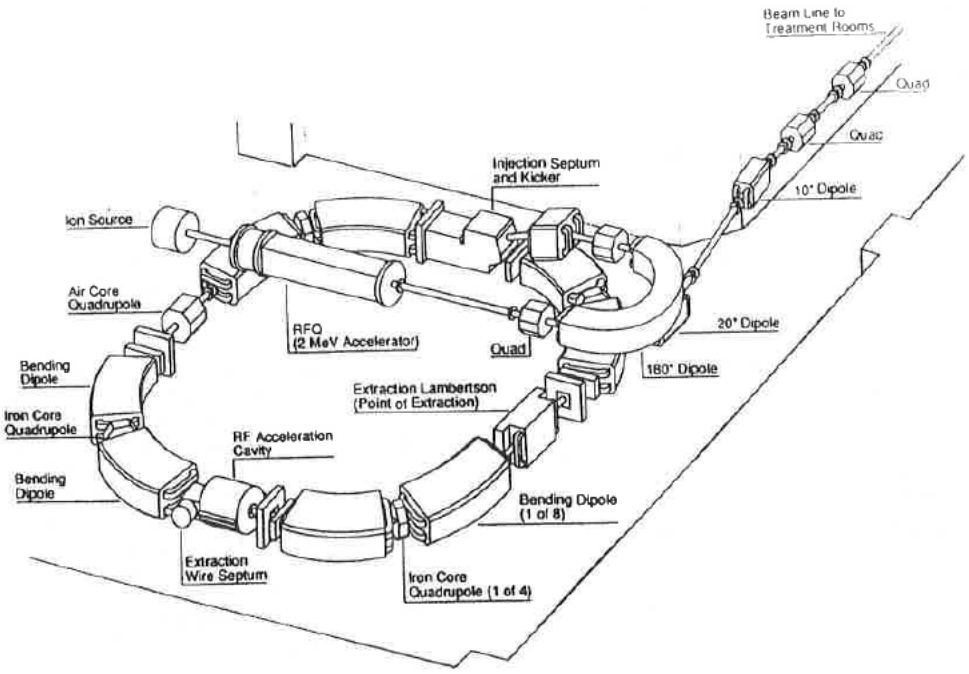

FIGURE 8–26. Variable-energy proton synchrotron for the Loma Linda cancer therapy facility. The air core quadrupole in the accelerator regulates beam extraction using the beam intensity monitoring signal from the treatment room. (Coutrakon G, Bauman M, Lesyna D, et al: A prototype beam delivery system for the proton medical accelerator at Loma Linda. Med Phys 18:1093–1099, 1991)

ment room with two horizontal beam delivery systems, and a fifth beam room for physics and biologic research. Proton beams are generated by a synchrotron designed and built by Fermi National Laboratory (Batavia, IL). Acceleration energy is continuously variable from 70 to 250 MeV.

Several other institutions provide proton treatment facilities outside the United States.[49] The Gustav Werner Institute in Upsala, Sweden, produces 185-MeV proton beams for radiation treatment using a cyclotron. In Russia, a 750-MeV beam is available from a synchrotron for proton treatment at the Institute for Theoretical and Experimental Physics in Moscow, and a 1-GeV synchrocyclotron is used for proton treatment at the Joint Institute for Nuclear Research in Dubna. A sector-focused cyclotron is used to produce 90-MeV proton beams for treatment at the National Institute for Radiological Science in Chiba, Japan. In Tsukuba, Japan, a synchrotron generates 250-MeV beams for proton treatment at the Particle Radiation Medical Center, and the Paul Scherrer Institute in Villigen, Switzerland, has a facility for proton treatment of the eye using 70-MeV beams from a synchrotron injector.

Neutron Beam Treatment Units

Most neutron radiation therapy in the past was performed either with nuclear physics cyclotrons that were only marginally suitable for radiation therapy applications because of their low-energy, stationary and fixed collimators, and non–hospital-based location, or with machines manufactured specifically for radiation therapy that do not meet modern standards (low energy, low output, unreliable). Modern neutron therapy machines, with proton and deuteron energies of about 50 MeV, produce neutron beams with depth-dose characteristics equivalent to about 6-MV x-rays.

Energy spectra for neutrons produced by four different mechanisms are shown in Fig. 8–27.[19] Fission neutrons, although suitable for neutron capture therapy, cannot be used for teletherapy because of their low energy and concomitantly poor penetration, so they will not be discussed further. The d-T reaction shown produces monoenergetic neutrons of energy 14 MeV, which is high enough to treat most deep-seated lesions.

$$^{2}_{1}\mathrm{d} + {}^{3}_{1}\mathrm{H} \rightarrow {}^{4}_{2}\mathrm{He} + {}^{1}_{0}\mathrm{n} + 17.6\ \mathrm{MeV}$$

The d-T generators are especially attractive because deuteron energies of only 0.2 MeV are needed, which makes the entire machine both inexpensive and compact, so that the entire unit can be mounted isocentrically. Unfortunately, several undesirable characteristics (low output, poor penetration, large penumbra, short target lifetime) of these generators have made them almost extinct as therapy machines.

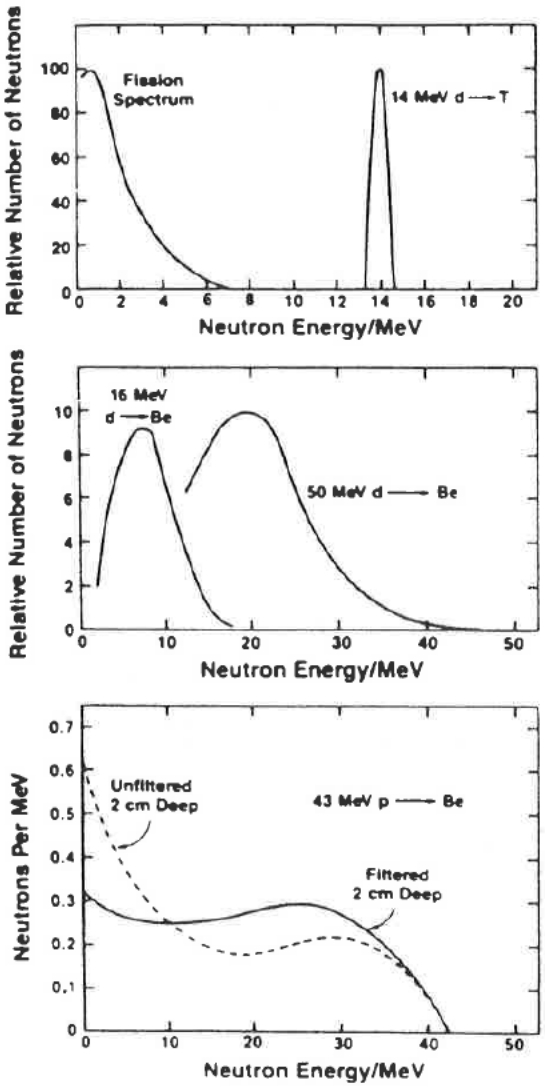

FIGURE 8–27. Neutron spectra for different beam production methods. (Hall EJ: Radiobiology for the Radiologist, ed 4. Philadelphia, JB Lippincott, 1994)

All the remaining neutron therapy machines are particle accelerators with neutron production based on p,Be, d,Be, or d,D interactions:

$$^{1}_{1}p + {}^{9}_{4}Be \rightarrow {}^{9}_{5}B + {}^{1}_{0}n - 18.5 \text{ MeV}$$

or

$$^{2}_{1}d + {}^{9}_{4}Be \rightarrow {}^{10}_{5}B + {}^{1}_{0}n + 3.79 \text{ MeV}$$

or

$$^{2}_{1}d + {}^{2}_{1}H \rightarrow {}^{3}_{2}He + {}^{1}_{0}n + 3.27 \text{ MeV}$$

The d,D reaction is rarely used for radiation therapy machines, however, because the kinetics of the reaction are such that the average energy of the neutrons from deuterons on deuterium is less than that for the d,Be reaction for deuteron energies above about 10 MeV. The p,Be reaction is most commonly used in modern isocentric neutron therapy machines. The main reasons that this reaction is preferred over d,Be are that proton accelerators are much smaller and less expensive than deuteron accelerators per average neutron energy, and proton beams are much easier to bend around the gantry of an isocentric unit. The only exception is the superconducting cyclotron installed at Harper Hospital in Detroit.[42] With superconducting technology, the entire cyclotron is small enough to be rotated around the patient on isocentric rings (Fig. 8–28), thus eliminating the need for bending the deuteron beam around a rotating gantry. Also, the neutron yield for the d,Be reaction is about five times that for p,Be.

Radiation Therapy Simulator

The historic development of the radiation therapy simulator is reviewed by Day and Harrison.[13] The modern simulator mimics the functions and allowed motions of a therapy unit and uses a diagnostic x-ray tube to simulate the radiation properties of the treatment beam (Fig. 8–29).[3,83] A simulator allows the beam direction and the treatment fields to be determined to encompass the target volume and to spare normal structures excessive radiation. Radiographic visualization of internal structures in relation to external landmarks allows special shielding devices to be constructed. Gantry arms are rigid enough to support heavy shielding blocks and simulated electron cones; couch widths are similar to therapy unit couch widths; and operating consoles feature digital displays of parameters and programmable settings for SAD, gantry angles, and field sizes. Most simulators are equipped with x-ray fluoroscopy to expedite field setup and beam angulations, and some units feature automatic exposure control for improved radiographic techniques. A brief update on selection, acceptance testing, and quality assurance is provided by McCullough.[45]

Computed Tomography (CT) Scanners and CT Simulators

The latest feature on conventional simulators uses the imaging device to record transmitted beam intensities as the simulator gantry rotates.[35,65] The resultant reconstructed images are analogous to conventional CT images. This is typically referred to as simulator-CT. Early simulator based scanners suffered from poor spatial resolution and poor images. However, the latest commercial simulator-CT systems produce images of acceptable quality, and in some sites of the body (head, neck, and lung) almost diagnostic quality images can be obtained.[39] One obvious advantage of such a device is its low cost as compared

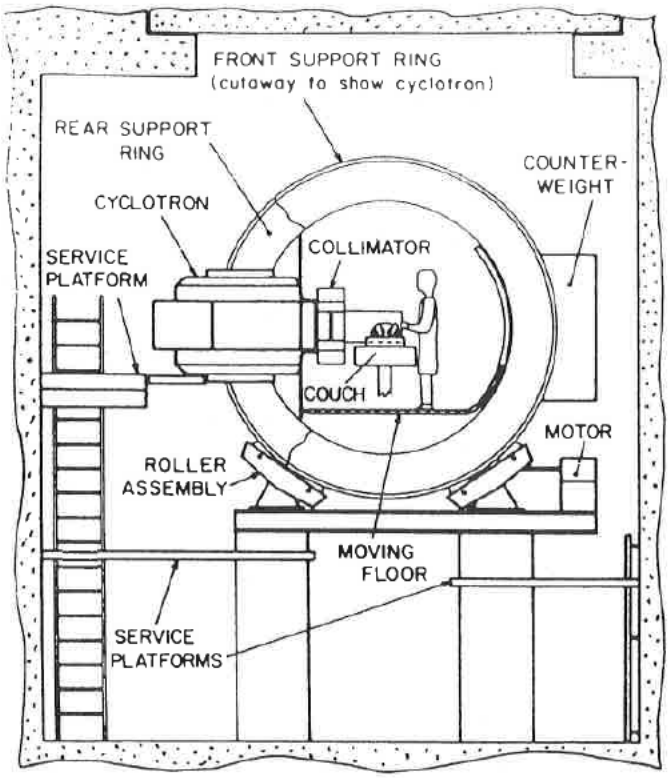

FIGURE 8–28. Cross-sectional drawing of the fully rotatable superconducting cyclotron system installed at the Gershenson Radiation Oncology Center of Harper Hospital, Detroit, Michigan. (Maughan RL, Powers WE: A superconducting cyclotron for neutron radiation therapy. Med Phys 21:779–785, 1994)

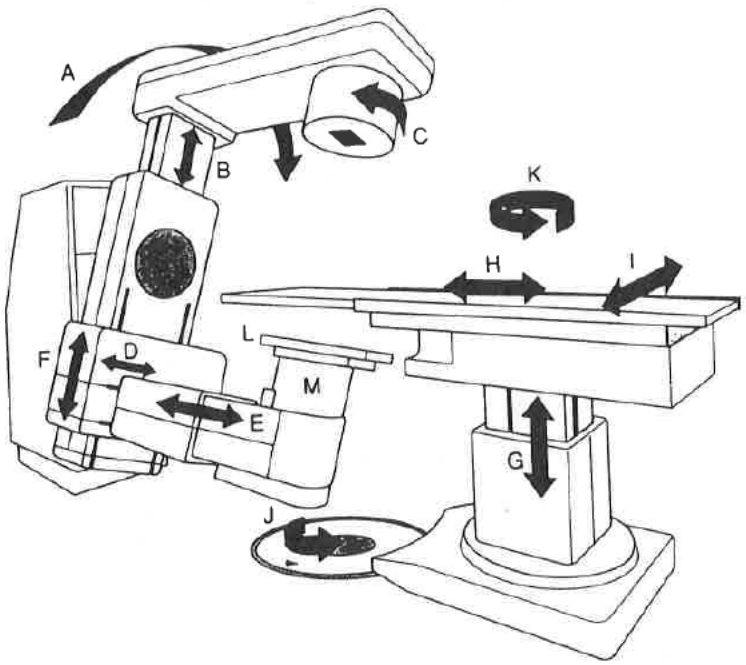

FIGURE 8–29. The basic components and motions of a radiation therapy simulator: A, gantry rotation; B, source-axis distance; C, collimator rotation; D, image intensifier (lateral); E, image intensifier (longitudinal); F, image intensifier (radial); G, patient table (vertical); H, patient table (longitudinal); I, patient table (lateral); J, patient table rotation about isocenter; K, patient table rotation about pedestal; L, film cassette; M, image intensifier. Motions not shown include field size delineation, radiation beam diaphragms, and source–tray distance. (Van Dyk J, Mah K: Simulators and CT scanners. In Williams JR, Thwaites DI, eds: Radiotherapy Physics. New York, Oxford Medical Publications, 1993)

with a CT scanner. In addition, the geometry of the simulation is more representative of the therapy machine geometry than is a diagnostic CT scanner; thus, patient setups produced by a simulator-CT unit are not as constrained as they are with conventional CT scanners with their limited scan tunnel sizes (70 cm). The disadvantages are the slow scan speed (which is not adequate for volumetric scans required for three-dimensional planning as discussed in Chapter 12) and, although improved, image quality, which is not comparable with that provided by modern spiral CT scanners.

This has led researchers and some manufacturers to integrate a CT scanner with features designed for radiation therapy with an advanced radiation therapy planning computer.[52,53,59,60,77,80] Such a system is referred to as a CT-simulator and provides many advanced image manipulation and viewing advantages including beam's eye view display, which allows the anatomy to be viewed from the perspective of the radiation beams and allows field shaping electronically at the graphics display station. A CT-simulator also introduces the concept of virtual simulation whereby the generation and comparison of beam's eye view digitally reconstructed radiographs can be performed in the absence of the patient.[67,73–75] Although some development work still remains (e.g., larger scan tunnel, improved image segmentation and correlation software), CT-simulators will likely render conventional simulators obsolete by the year 2000.

QUALITY OF RADIATION

From the physical standpoint, the quality (i.e., penetrability) of any ordinary x-ray beam is completely specified by its spectral distribution curve, which is based on the relative intensities of photons of various energies and is a result of fluctuations of tube potential, the bremsstrahlung radiation process, characteristic radiation, and multiple interactions of the incident electrons and the x-ray target.

Figure 8–30 shows a typical spectral distribution curve for a photon beam. The distribution of the photon energies, including the peak photon energy, in the continuous spectrum is governed solely by the x-ray tube potential. However, the energy of the characteristic photons increases with increasing atomic number of the target element. All other factors being equal, the radiation intensity is proportional to the atomic number of the target element.

Spectral distribution of an x-ray beam can be modified by placing absorbing materials of various thickness (i.e., filters) in the beam. In general, a filter removes relatively more low-energy photons than high-energy photons, although photons of all energies are removed to some extent. For radiation in the orthovoltage region (except for the absorption edge effect), the lower the energy of the photons, the larger the total mass attenuation coefficient, and therefore the greater the likelihood that the photon

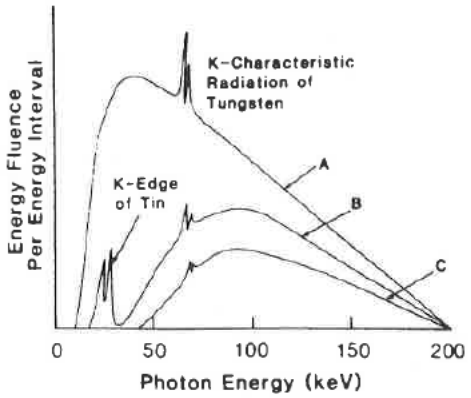

FIGURE 8–30. Schematic graph showing spectral distribution of 200-kVp x-ray beam with different added filters. (Khan FM: The Physics of Radiation Therapy, ed 3. Baltimore, Williams & Wilkins, 1994)

will be absorbed. Therefore, the beam emerges from the filter with a larger percentage of high-energy photons than it had on entering the filter. This beam has a greater penetration power and is said to have been "hardened" by the filter. The quality of an x-ray beam improves with increasing tube potential and with increasing thickness and atomic number of the filter.

A specification of beam quality based entirely on a spectral distribution is too cumbersome for radiation therapy. The usual method of specifying beam quality in superficial and orthovoltage therapy is involves indicating the HVL and the accelerating potential. For megavoltage beams, only the maximum energy of the electrons striking the x-ray target is typically used. The homogeneity coefficient denotes how homogeneous an x-ray beam is with respect to its photon energies. It is defined as the ratio of the first HVL to the second. As the filtration is increased, the exposure rate decreases; therefore, there is a practical limit of filter thickness in orthovoltage therapy with a given combination of kilovolts, milliamperes, and distance. In certain situations it is convenient to express the quality of the x-ray beam in terms of an "equivalent energy," which can be derived from knowledge of the HVL. The type of x-ray beam that is used in radiation therapy is always heterogeneous, consisting of many different energies; however, the beam can be considered to have a definite equivalent energy if monoenergetic radiation of that energy has the same HVL as the radiation in question.

RADIATION EXPOSURE

In 1928, at the Second International Congress of Radiology, the ionization of air, called exposure, was adopted as the measurable effect of radiation of a photon beam.[50] As the beam passes through a material, it creates ion pairs

Principles and Practice of Radiation Oncology, Third Edition, edited by C. A. Perez and L. W. Brady. Lippincott–Raven Publishers, Philadelphia © 1997.

CHAPTER 9

External Photon Beam Dosimetry and Treatment Planning

James A. Purdy and Eric E. Klein

When treating a patient with cancer, the radiation oncologist is faced with the problem of prescribing a treatment regimen with a radiation dose that is large enough to potentially cure or control the disease but does not cause serious normal tissue complications. This task is a difficult one because tumor control and normal tissue effect responses are typically steep functions of radiation dose; that is, a small change in the dose delivered (±5%) can result in a dramatic change in the local response of the tissue (±20%).[34,53,54,142] Moreover, the prescribed curative doses are often, by necessity, very close to the doses tolerated by the normal tissues. Thus, for optimum treatment, the radiation dose must be planned and delivered with a high degree of accuracy.

As explained in Chapter 8, we can readily compute the dose distribution from radiation beams of photons, electrons, or mixtures of these impinging on a regularly shaped, flat-surface, homogeneous unit density phantom. However, the patient presents a much more complicated situation because of irregularly shaped topography and many tissues of varying densities and atomic composition (called heterogeneities). In addition, beam modifiers, such as wedges and compensating filters or bolus, are sometimes inserted into the radiation beam to achieve the desired dose distribution. Dose computational algorithms that completely account for the complex geometries, heterogeneities, and beam modifiers are not yet practical for radiation treatment planning systems (but are likely to be by the next decade), and instead correction factor–type algorithms that approximate the situation are used (see Chapter 8).

In this chapter, we review several aspects of clinical photon beam dosimetry, including the effects of patient topography and internal heterogeneities on dose distributions of radiation beams and typical irradiation techniques. In addition, we consider the treatment planning process including simulation, treatment aids, verification of treatment delivery, and related quality assurance (QA) issues. We stress fundamental concepts and include references for the most recent applications or technologies using these concepts.[8,52,58,69,118,131,141,156,157,162]

CLINICAL PHOTON BEAM DOSIMETRY

Single-Field Isodose Distributions

As explained in Chapter 8, the central-axis percentage depth dose (PDD) expresses the penetrability of a radiation beam. Table 9–1 summarizes beam characteristics for x-ray and γ-ray beams typically used in radiation therapy and lists the depth at which the dose is maximum (100%) and the PDD value at a depth of 10 cm. Representative PDD curves are shown in Fig. 9–1 for conventional source-to-skin distances (SSDs). As a rule of thumb for a 10 × 10 cm field, 18-MV and 6-MV x-ray beams, as well as ^{60}Co (1.25-MV average x-ray energy) beams lose approximately 2%, 3.5%, and 4.5% per cm, respectively, beyond the depth of maximum dose, d_{max}. Because x-ray beams with an energy greater than 18 MV are not widely used in radiation therapy, we limit our discussion to this and lower energies. There is no agreement on a single optimal x-ray beam energy; instead, its selection is typically influenced by institutional bias or radiation oncologist training, and it is generally treatment site specific.

Isodose charts, such as those shown in Fig. 8–42, provide much more information about the radiation beam than the central-axis PDD alone. However, isodose charts represent the dose distribution in only one plane (typically the one containing the beam's central axis) and are usually available only for square or rectangular fields.

Isodose charts are generally measured with the radiation beam directed perpendicular to a water phantom with

TABLE 9–1. *Beam characteristics for photon beam energies of interest in radiation therapy*

200 kVp, 2.0 mm Cu HVL, SSD = 50 cm
Depth of maximum dose = surface
Rapid fall off with depth due to (1) low energy and (2) short SSD
Sharp beam edge due to small focal spot
Significant dose outside beam boundaries due to Compton scattered radiation at low energies
^{60}CO, SSD = 80 cm
Depth of maximum dose = 0.5 cm
Increased penetration (10 cm %DD = 55%)
Beam edge not as well defined—penumbra due to source size
Dose outside beam low since most scattering is in forward direction
Isodose curvature increases as the field size increases
4-MV x-ray, SSD = 80 cm
Depth of maximum dose = 1.0–1.2 cm
Penetration slightly greater than cobalt (10 cm %DD = 61%)
Penumbra smaller
"Horns" (beam intensity off-axis) due to flattening filter design can be significant (14%)
6-MV x-ray, SSD = 100 cm
Depth of maximum dose = 1.5 cm
Slightly more penetration than ^{60}Co and 4 MV (10 cm %DD = 67%)
Small penumbra
"Horns" (beam intensity off-axis) due to flattening filter design reduced (9%)
18-MV x-ray, SSD = 100 cm
Depth of maximum dose = 3.0–3.5 cm
Much greater penetration (10 cm %DD = 80%)
Small penumbra
"Horns" (beam intensity off-axis) due to flattening filter design reduced (5%)
Exit dose often higher than entrance dose

a flat surface and uniform density. When the dose distribution is calculated for a patient whose surface is rarely flat and whose internal density is never uniform, the isodose chart is corrected for the effects of irregular surface topography, oblique incidence, and inhomogeneities encountered in the path of the beam, as discussed in Chapter 8.

The isodose curves shown in Fig. 8–42 show the relative uniformity of the beams at depth and the dose distributions in the penumbra region for different beam energies. Cobalt units exhibit a large penumbra, and their isodose distributions are rounded toward the source as a result of the relatively large source size (typically 1 to 2 cm in diameter). Linear accelerator (linac) isodose distributions have much smaller penumbra and relatively flat isodose curves at depth. However, they typically exhibit greater beam intensity away from the central axis, the so-called horns, at shallow depths, particularly at d_{max}. In general, each therapy unit has unique dosimetry features, and isodose distributions should be measured for each unit.

The radiation field size, the dimensions of the radiation beam perpendicular to its direction of incidence, corresponds to the 50% isodose at the beam's edge and is stated at the skin surface for SSD treatments and at the axis depth for source-to-axis distances (SADs) for isocentric treatments.

Build-up Region

When a photon beam strikes the tissue surface, electrons are set in motion, causing the dose to increase with depth until the maximum dose is achieved at depth d_{max}. Figure 8–38 shows the build-up of dose with depth beneath the entry surface for common photon energies. As the energy of the photon beam increases, the depth of the build-up region is increased. The subcutaneous tissue-sparing effects of these higher energy x-rays, combined with their great penetrability, make them well suited for treating deep lesions. For a specific x-ray energy, the magnitude of the skin dose generally increases with field size and the addition of plastic blocking trays (Fig. 9–2). Plastic blocking trays should be at least 20-cm above the skin surface because skin doses are increased for lesser distances. Copper, lead, or lead glass filters beneath plastic trays can be used to remove the undesired

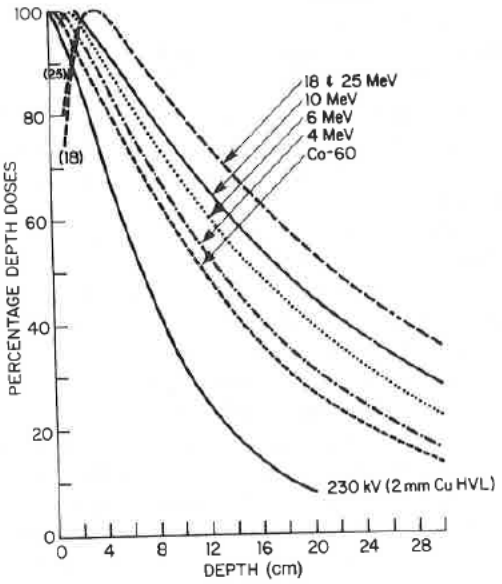

FIGURE 9–1. Typical x-ray or photon beam central-axis percentage depth dose curves for a 10 × 10 cm beam for 230 kV (2-mm Cu HVL) at 50-cm SSD, ^{60}Co and 4 MV at 80-cm SSD, and 6 MV, 10 MV, 18 MV, and 25 MV at 100-cm SSD. The latter two beams coincide at most depths but do not coincide in the first few millimeters of the build-up region. The 4-MV, 6-MV, 18-MV, and 25-MV data are for the Varian Clinac 4, 6, 20, and 35 units, respectively, at the Mallinckrodt Institute of Radiology in St. Louis. (Cohen M, Jones DEA, Greene D: Central axis depth dose data for use in radiotherapy. Br J Radiol 11:21[suppl], 1972)

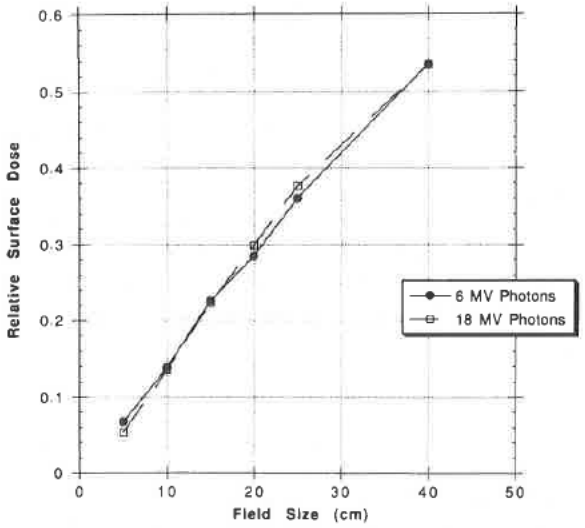

FIGURE 9–2. Relative surface dose versus field size with blocking tray in place for 6-MV and 18-MV photons. (Klein EE, Purdy JA: Entrance and exit dose regions for Clinac-2100C. Int J Radiat Oncol Biol Phys 27:429–435, 1993)

lower energy electrons that contribute to skin dose, but this is rarely done in the clinic.[117,129]

As shown in Fig. 9–3, if the x-ray beam is incident normal (at 0 degrees) to the surface, maximum skin sparing is achieved. Skin dose increases as the angle of incidence increases because more secondary electrons are ejected along the oblique path of the beam.[40,44,62,145] As the angle of the incident radiation beam increases, the surface dose increases, and d_{max} moves toward the surface.

Exit Dose Region

The skin and superficial tissue on the side of the patient from which the beam exits receive a reduced dose if sufficient backscatter material is not present. The amount of dose reduction is a function of x-ray beam energy, field size, and the thickness of tissue that the beam has penetrated reaching the exit surface. Gagnon and Grant[39] measured a 16% reduction in dose at a depth of 0.01 mm for a cobalt beam penetrating either 7.7 or 15 cm of tissue. At 1 mm from the exit surface, the dose was reduced by 8% for a 30 × 30 cm field but only 3% to 4% for a 6 × 6 cm field. For a 6-MV beam, Purdy[117] measured a 15% reduction in dose with little dependency on field size. This work was repeated for 18-MV beams by Klein and Purdy,[76] who found an 11% reduction in exit dose.

Generally, the addition of a thickness of tissue-equivalent material on the exit side equivalent in thickness to about two thirds of the d_{max} depth is sufficient to provide full dose to the build-down region on the exit side. Figure 9–4 shows the effects of various backscattering media when placed directly behind the exit surface.[76]

Patient Heterogeneities

When dose is calculated in the patient during treatment planning, measured water dosimetry data can be corrected for the presence of tissue inhomogeneities, such as the lungs, bony structures, air cavities, and prostheses. The change in dose is due to the perturbation of the transport of primary and scattered photons and that of the secondary electrons set in motion from photon interactions. Depending on the energy of the photon beam and the shape, size, and constituents of the inhomogeneities, the resultant change in dose can be large.

Perturbation of photon transport is more noticeable for lower energy beams. There is usually an increase in transmission, and therefore dose, when the beam traverses a low-density inhomogeneity. The reverse applies when the inhomogeneity has a density higher than that of water. However, the change in dose is complicated by the concomitant decrease or increase in the scatter dose. For a modest lung thickness of 10 cm, there will be about 15% increase in the dose to the lung for a ^{60}Co or 6-MV x-ray beam,[22] but only about 5% for an 18-MV x-ray beam[95] (Fig. 9–5).

When there is a net imbalance of electrons leaving and entering the region near an inhomogeneity, the condition of electron equilibrium is disrupted. The effects are similar to those in the build-up region, near a beam edge, or in a small beam. Because electrons have finite travel, the resultant change in dose is usually local to the vicinity of the inhomogeneity and may be quite large. The effects are more noticeable for the higher energy photon beams due to the increased energy and range of the scattered electron. Near the edge of the lungs and air cavities, the reduction in dose can be larger than 15%.[79] For inhomogeneities with density larger than water, there will be an increase in dose locally due to the generation of more electrons. However, most dense inhomogeneities have atomic numbers higher than that of water so that the

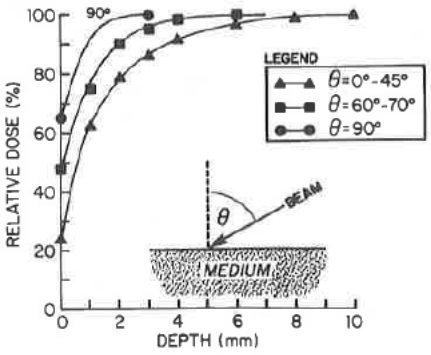

FIGURE 9–3. The variation of surface dose and depth of maximum dose as a function of the angle of incidence of the x-ray beam with the surface (4 MV, 10 × 10 cm).

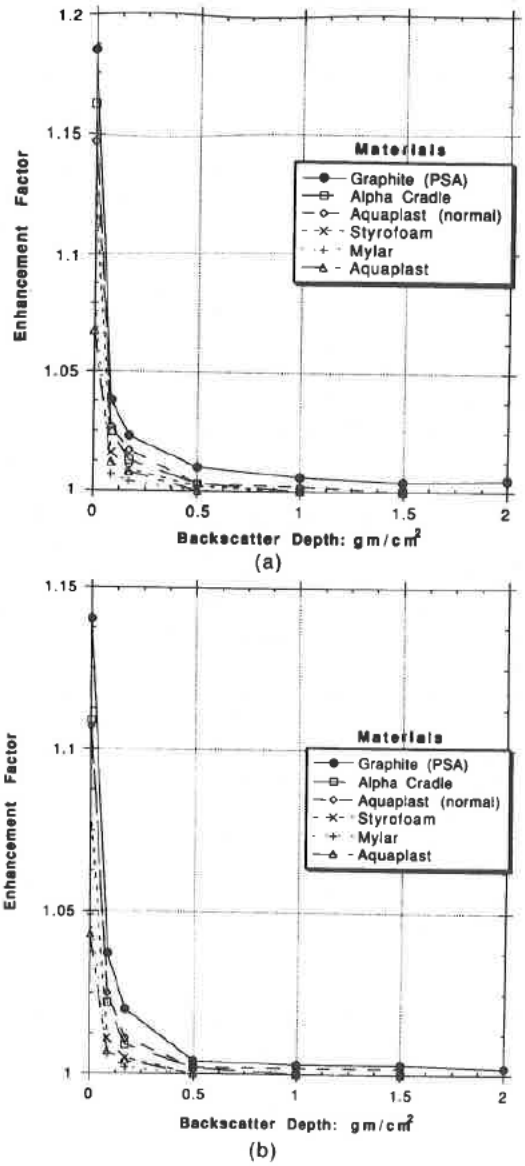

FIGURE 9–4. Enhancement of exit dose for (**A**) 6-MV and (**B**) 18-MV photons for a 15 × 15 cm field at 100 cm SAD versus backscatter depth for various backscattering materials. (Klein EE, Purdy JA: Entrance and exit dose regions for Clinac-2100C. Int J Radiat Oncol Biol Phys 27:429–435, 1993)

resulting dose perturbation is further compounded by the perturbation of the multiple coulomb scattering of the electrons. Near the interface between a bony structure and waterlike tissue, large hot and cold dose spots can be present.

At present, clinical inhomogeneity correction methods address only the problem of photon transport. As a result, treatment plan dose calculations tend to show that the effects of inhomogeneities are reduced with increasing photon energies. Even when only photon transport is perturbed, the present methods are only approximate and have inadequacies. For the future, emphasis should be placed on implementing more advanced and accurate methods for clinical use.[14,94,96,103] However, for the next few years, clinical dose calculations will likely still be based on the methods discussed in Chapter 8. The clinical physicist should take proper precautions, such as verifying with measurements, in situations in which inaccuracies could lead to an undesirable clinical outcome.

Interface Dosimetry

Measurements within the body at transition zones (interfaces) of different media may have large uncertainties associated with them. The central-axis doses in these regions depend on radiation field size (scatter influence), distance between interfaces (e.g., air cavities), differences between physical densities and atomic number of the interfacing media, and the size and shape of the different media.

Measurements are generally done with parallel-plate ionization chambers. Corrections should be used to account for plate separation, energy (ionization ratio), and guard width.[45,153] Thermoluninescent dosimeters (TLDs) and film also have been used for transition zone measurements, but the problems associated with thickness and atomic number (respectively) and the associated QA needed make measurements with these dosimeters more laborious, and the results typically have a greater uncertainty. Many benchmark measurements have been re-

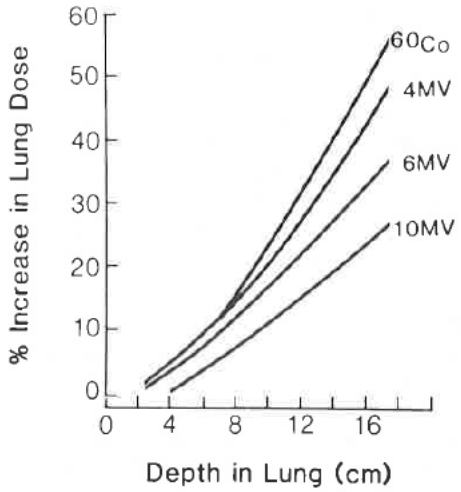

FIGURE 9–5. Percentage increase in lung dose as a function of depth in the lung for selected energies. Field size is 10 × 10 cm. (Reprinted with permission from McDonald SC, Keller BE, Rubin P. Method for calculating dose when lung tissue lies in the treatment field. Med Phys 3:210, 1976)

ported for various geometries simulating clinical situations such as air cavities (larynx), lung (mediastinum), bone (femur), and prostheses (steel for hip and silicon for breast); their clinical impact is discussed below.

Air Cavities

Many investigators have made measurements for air cavities over an energy range from ^{60}Co to 15-MV x-rays. Epp and colleagues[33] performed measurements with a parallel-plate ionization chamber for cobalt that showed significant losses of ionization on the central axis after air cavities of varying dimensions. The losses, which were due to lack of forward scattered electrons, were approximately 12% for a typical larynx air cavity but were recovered within 5 mm in the new build-up region. Koskinen and Spring[80] confirmed these measurements with ultrathin (20 mm) LiF-Teflon dosimeters and reported similar responses in the proximal region of the air cavity due to lack of backscatter. Nillson and Schnell[110] used even thinner LiF disks (10 mm) and found further loss for ^{60}Co in both the proximal and distal regions. They also presented data for 6- and 42-MV photons, with the higher-energy beam showing fewer effects. Epp and colleagues[32] measured a 14.5% loss at the distal interface for 10-MV photons with a build-up curve that plateaued within 20 mm of the interface. Beach and associates[7]

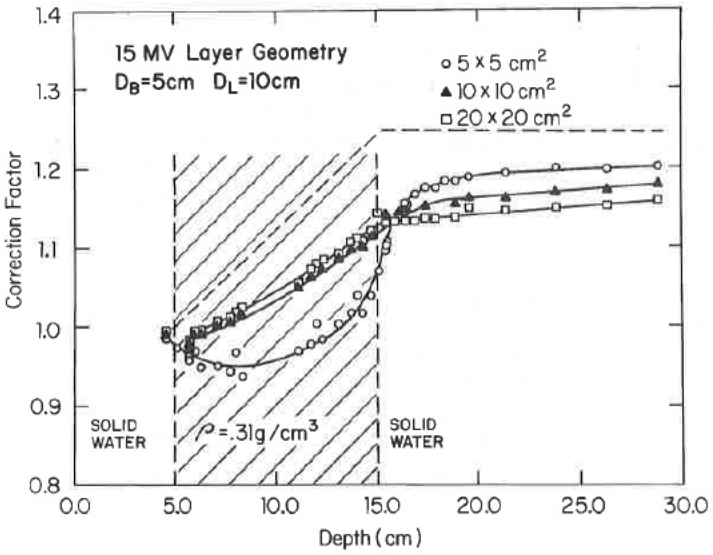

A

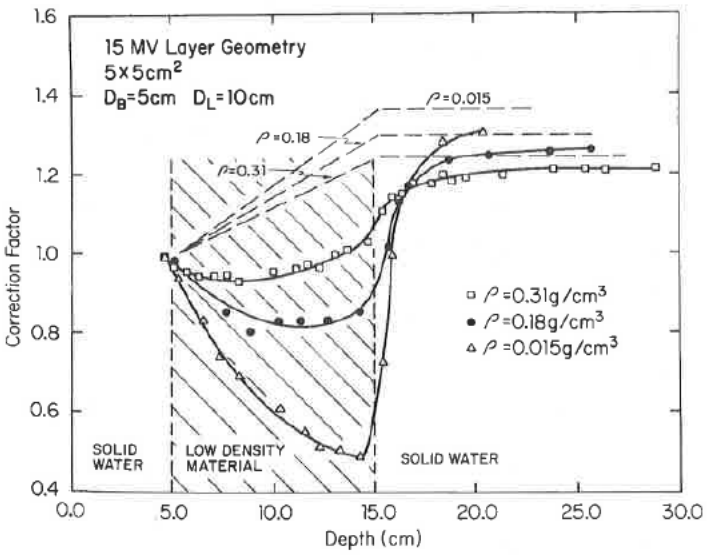

B

FIGURE 9–6. Dose perturbation factor at tissue-lung interface for 15-MV x-rays: (**A**) for varying field size and (**B**) for varying lung density. (Rice RK, Mijnheer BJ, Chin LM: Benchmark measurements for lung dose corrections for x-ray beams. Int J Radiat Oncol Biol Phys 15:399–409, 1988)

measured losses at the distal interfaces with an extrapolation chamber and recommended minimum field sizes to be used in irradiation of the larynx to balance losses due to forward scatter. Klein and colleagues[71] measured distributions about air cavities for 4-MV and 15-MV photons with a parallel-plate chamber in both the distal and proximal regions. They combined the distributions in a parallel-opposed fashion and observed a 10% loss at the interfaces for an air cavity of 2 × 2 × 20 cm for 4 × 4 cm parallel-opposed fields for either energy. They also observed losses at the lateral interfaces perpendicular to the beam on the order of 5% for the 4-MV beam.

Lung Interfaces

Although the problem of reestablishing equilibrium is not as severe as with air cavities, a transition zone region at the lung–tissue interface still exists over the range of clinical photon beam energies. Rice and colleagues[125] measured responses within various simulated lung media using a parallel-plate chamber and phantom constructed of simulated lung material. The constructed average lung material (ρ = 0.31 g/cm^3) contained balsa wood for low-density lung (ρ = 0.18 g/cm^3) and foam for a low-end lung material (ρ = 0.015 g/cm^3). They measured correction factors (CFs) with a 10-cm layer of lung material versus water and observed minor differences at the interface compared with regions beyond the lung and a small dependence on field size (7% for 4 MV) (Fig. 9–6A). A considerable build-up curve was observed (10% change in CF) for a 5 × 5 cm field for the 15-MV beam, which began in the distal region of the lung and plateaued beyond the lung (Fig. 9–6B). The central axis PDD showed a minor dependence on the lateral extent of the lung, but a substantial change due to the difference in physical densities. For the 4-MV 5 × 5 cm beam, a gradient of 40% from the interface to the equilibrium region was measured following the foam media. The 15-MV 5 × 5 cm beam exhibited a 30% gradient following balsa and a 60% gradient following the foam region. Only a 2% CF was measured in the proximal region.

Bone Interfaces

Das and colleagues[23,24] measured dose perturbation factors (DPFs) proximal and distal for simulated bone–tissue interface regions using a parallel plate chamber for both 6- and 24-MV beams. They reported DPFs of 1.1 for the 6-MV beam and 1.07 for the 24-MV beam at the proximal interface. A 7% enhancement (build-down) was measured for the 24-MV beam at the distal interface, whereas the 6-MV beam exhibited a new build-up region distally with a DPF of 0.95 at the interface. Klein and co-workers[71] made similar measurements for 4- and 15-MV photons with similar results except that the 15-MV beam exhibited no enhancement. These build-up or build-down regions dissipated within a few millimeters in the tissuelike media. The perturbations were independent of thickness and lateral extent of the bone or radiation field size.

Prostheses (Steel and Silicon)

Das and associates[23] measured forward dose perturbation factors (FDPFs) following a 10.5 mm thick stainless-steel layer simulating a hip prosthesis geometry. They measured an enhancement of 19% for 24-MV photons and 3% for 6-MV photons. They also measured backscatter dose perturbation factors (BDPFs) for various energies for many high-Z materials including steel. They observed an enhancement of 30% for steel due to backscattered electrons independent of energy, field size, or lateral extent of the steel. These interface effects dissipated within a few millimeters in polystyrene. Other reports dealing with dosimetry perturbations due to metal objects are included in the references.[135,148]

Klein and Kuske[73] reported on interface perturbations about silicon prostheses. Such prostheses have a density similar to breast tissue but have a different atomic number. They observed a 6% enhancement at the proximal interface and a 9% loss at the distal interface.

Wedge Filter Dosimetry

When a wedge filter is inserted into the beam, the dose distribution is angled at some specified depth to some desired angle relative to the incident beam direction over the entire transverse dimension of the radiation beam (Fig. 9–7). For cobalt units, the depth of the 50% isodose

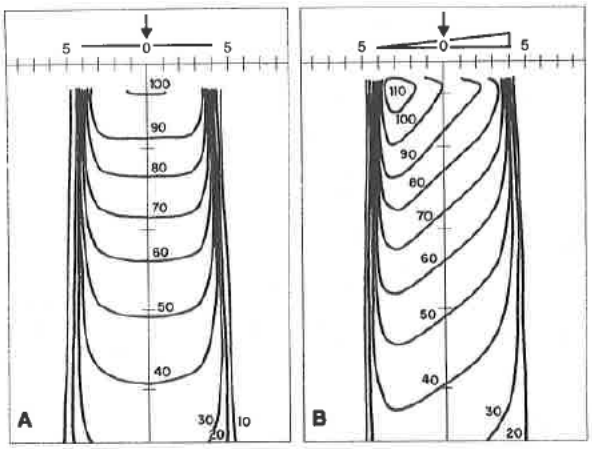

FIGURE 9–7. Isodose distributions for a 6-MV x-ray beam with an 8 × 8 cm field size. (**A**) Open field. (**B**) Field with a 45-degree wedge. (Khan FM: The Physics of Radiation Therapy, ed 3. Baltimore, Williams & Wilkins, 1994)

is usually selected for specification of the wedge angle, whereas for higher energy linacs, higher percentile isodose curves, such as the 80% curve, or the isodose curves at a specific depth (10 cm) are used to define the wedge angle. To understand the principles involved in designing a wedge filter, a stepwise review of the manual process is listed below and illustrated in Fig. 8–44.

1. A reference line is drawn at the depth selected to specify the wedge angle across the nonwedged isodose chart perpendicular to the central axis.
2. Fan lines at fixed intervals are drawn on both sides of the central axis.
3. A series of lines are drawn parallel to one another, making an angle with the central axis equal to the complement of the wedge angle and intersecting the central axis at the same points of intersection as the nonwedge isodose lines.
4. A table is constructed listing the nonwedge isodose values and the wedge isodose values for the points of intersection of each fan line and the reference line.
5. The ratio of the wedge isodose value to the nonwedge isodose value for each intersection point is calculated, and the ratios are renormalized to the largest value within the irradiation field to give the relative transmission ratio for each fan line.
6. The wedge filter can then be constructed from an appropriate material to give the transmission values determined in step 5.

Cobalt unit wedges are typically designed for specific field sizes (nonuniversal wedges) to keep the dose rate of the unit within a useful clinical range. Linacs are typically equipped with multiple wedges (universal wedges) that may be used with an allowed range of field sizes. Some newer linacs feature a single wedge, an autowedge, and the desired wedge angle is obtained by the proper combination of wedged and unwedged treatment.

Although wedges can be designed for any desired angle, 15-, 30-, 45-, and 60-degree wedges are most common. The wedged isodose curves can be normalized in two ways, as shown in Fig. 9–8. In some older systems, the wedge dose distributions have the wedge factor (i.e., the ratio of the measured central axis dose rate with and without the wedge in place) incorporated into the wedged isodose distribution. More commonly, the wedge isodose curves are normalized to 100% at d_{max}, and a separate wedge factor is used to calculate the actual treatment

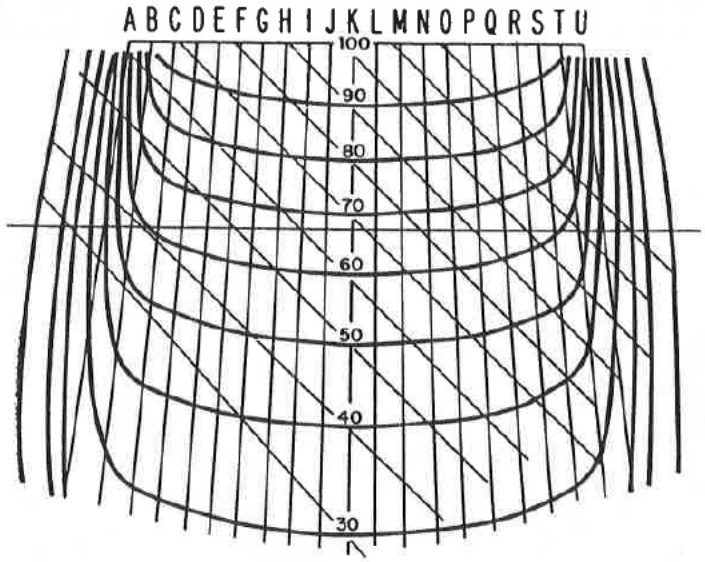

Transmission Ratios for the Construction of Wedge Filter

	A	B	C	E	G	I	K	M	O	Q	S	T	U
Nonwedge isodose	40	55	62	65	67	68	68	68	67	65	62	55	40
Wedge isodose	35	39	41	47	53	60	68	76	86	95	105	110	115
Ratio/wedge nonwedge	0.875	0.710	0.660	0.720	0.790	0.880	1.00	1.12	1.28	1.46	1.70	1.20	2.88
Transmission ratio			0.387	0.425	0.462	0.515	0.59	0.66	0.75	0.86	1.0		
mm Pb			15.2	13.6	12.2	10.5	8.3	6.5	4.5	2.3	0		

FIGURE 9–8. Method used for the design of a wedge filter. (Redrawn from Aron BS, Scapicchio M: Design of universal wedge filter system for a cobalt 60 unit. Am J Roentgenol 96:70, 1966)

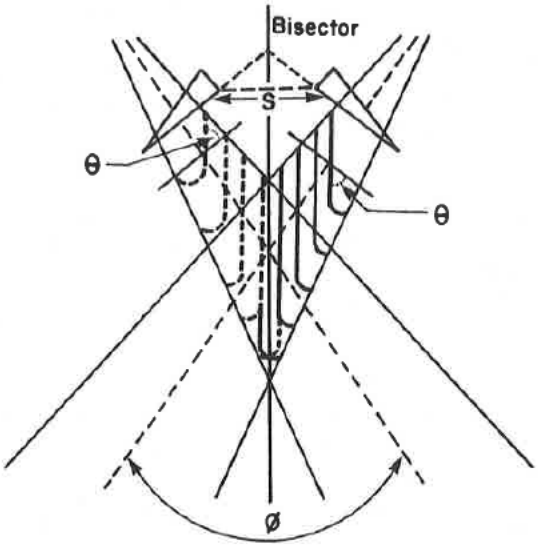

FIGURE 9–9. Parameters of the wedge beams: θ is the wedge angle, ϕ is the hinge angle, and S is separation. Isodose curves for each wedge field are parallel to the bisector. (Khan FM: The Physics of Radiation Therapy, ed 2. Baltimore, Williams & Wilkins, 1994)

monitor units or time. The inclusion or noninclusion is an extremely important point to understand as serious error in dose delivered to the patient can occur if used improperly. McCullough and associates[100] noted that wedge factors are generally correct to 2% to 10-cm depth, and at greater depths the wedge factors defined at d_{max} are accurate to 5% or less.

Sewchand and colleagues[130] and Abrath and Purdy[1] pointed out that beam hardening results when a wedge is inserted into the radiation beam. The percent depth dose (PDD), therefore, can be considerably increased at depth. Differences reported were nearly 7% for 4-MV 60-degree wedge field PDD from the open field PDDs at 12-cm depth and 3% difference in depth dose values between the wedge field and the open field for a 60-degree wedge using 25-MV x-rays.

When the patient's treatment is planned, wedged fields are commonly arranged such that the angle between the beams, the hinge angle ϕ, is related to the wedge angle θ by the following relationship (Fig. 9–9):

$$\theta = 90 \text{ degrees} - \phi/2.$$

For example, as shown in Fig. 9–10, 45-degree wedges orthogonal to one another yield a uniform dose distribution.

In the early 1990s, manufacturers of computer-controlled medical linacs introduced software to create a wedge-shaped distribution, typically referred to as dynamic wedge.[84] Under computer control, one collimator jaw is moved across the field in conjunction with adjustment of the dose rate over the course of one treatment. This technology provides superior dose distributions and eliminates the above-mentioned beam-hardening problem.[74]

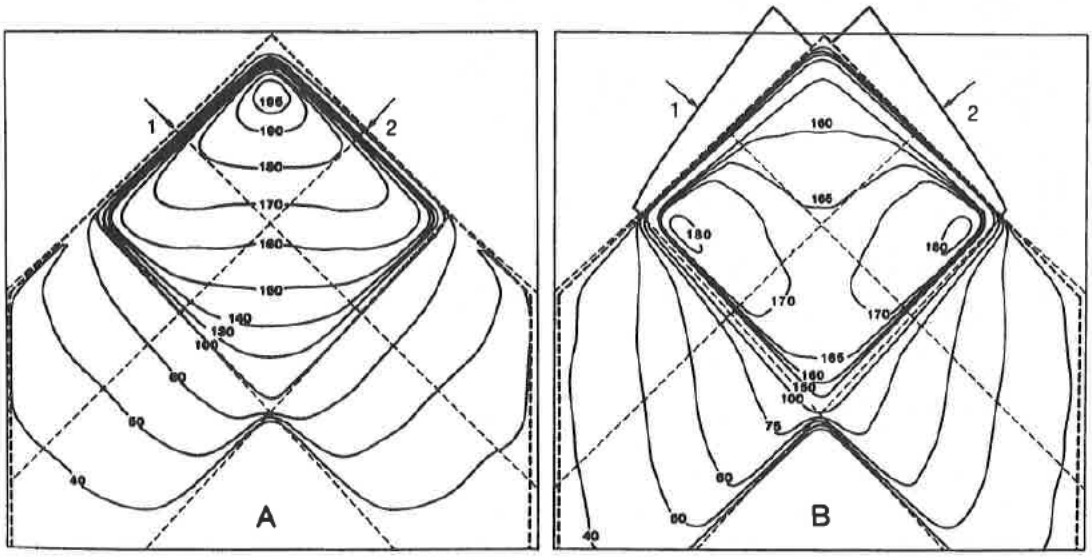

FIGURE 9–10. Isodose distribution for two angle beams. (**A**) Without wedges. (**B**) With wedges. 4-MV, field size = 10 × 10 cm, SSD = 100 cm, wedge angle = 45 degrees. (Khan FM: The Physics of Radiation Therapy, ed 2. Baltimore, Williams & Wilkins, 1994)